High-Resolution Geophysical Characterization of an Ethanol Release into an Existing Gasoline-Impacted Zone

by

John Mosquera

A thesis
presented to the University of Waterloo
in fulfillment of the
thesis requirement for the degree of
Master of Science
in
Earth Sciences

Waterloo, Ontario, Canada, 2012

Author's Declaration

I hereby declare that I am the sole author of this thesis. This is a true copy of the thesis, including any required final revisions, as accepted by my examiners.

I understand that my thesis may be made electronically available to the public.

John Mosquera

Abstract

This study aims to evaluate the ability of high-frequency (450 and 900 MHz) ground-penetrating radar (GPR) to monitor the effects of an ethanol release over an existing gasoline-contaminated zone. In September 2009, 184L of denatured ethanol mixture (E95) was released into an unconfined sand aquifer directly over gasoline residuals (E10) released the previous year. GPR profiling prior to the ethanol release indicated that the residual gasoline-contaminated zone was largely confined to its initial release point. The GPR profiling performed post ethanol release observed strong shallow reflection events which propagated laterally away from the trench over a one-month period, at which point the maximum extent was established. The effects of the ethanol were also observed with the 450MHz frequency, in the form of an apparent "velocity pull-up" of a stratigraphic reflector. After the initial expansion, reduction in reflection amplitude and increasing traveltimes within the trench, were observed until the onset of winter conditions and the development of frozen soil.

Over the winter the presence of ethanol inhibited the freezing process of the pore water in the contaminated zone, thus resulting in a difference in the dielectric properties of the unfrozen verse frozen zone. The unfrozen zone was significantly greater than the spatial extent of the strong reflection events that were monitored through GPR prior to winter. The spatial extent and depth of the unfrozen zone imaged by the GPR profiling was confirmed by a physical impedance depth survey. After thaw, evidence of the ethanol or gasoline was absent until mid-summer, when the water table dropped to approximately 80cm. At this point strong reflection events were again observed throughout the contaminated zone.

Acknowledgements

I would like to thank my family and friends, especially my parents Elsie and Chester Mosquera, who have supported me throughout the entirety of my education. Additionally I would like to thank Ulanna Wityk, and my two best friends Rob Rappolt and Adam Vuylsteke, who have had to endure me throughout this entire process.

I would like to convey my gratitude towards my supervisor Dr. Tony Endres, who throughout the entirety of this project provided support, either; academic, technical, or in the form of caffeine. I would like to thank Jim Barker for the opportunity to work on this project, and Juliana Freitas for answering my many questions. I would also like to thank the members of my committee; Jon Paul Jones and Jim Barker, for their thorough review and constructive comments which have undoubtedly improved the quality of this thesis. Thank you to Tom Edwards who most generously agreed to sit in for Jim Barker during the defence.

Thank you again to Juliana Freitas who was instrumental in the completion of this project. Throughout the entire process she was there to assist me either with field work at Borden, or presentations in Massachusetts. I wish you all the best with your position as a Professor in Brazil.

Also I'd like to thank my officemates and friends Colby Steelman, Melissa Bunn, Cameron Toy, and Cameron McNaughton for their valuable suggestions and comments. Over coffee or beer, in the field or in the lab, their assistance was always appreciated.

Table of Contents

List of Figures

List of Tables

1.0 Introduction

Contamination by immiscible organic liquids, also referred to as non-aqueous phase liquids (NAPLs), is widely recognized as a serious global groundwater quality issue (Domenico and Schwartz, 1998). While the solubility of these substances are typically low (e.g., polycyclic aromatic hydrocarbons or BTEX), the low concentrations needed to impact large scale water quality make NAPLs a significant groundwater threat (Corseuil et al., 2004).

NAPLs can be divided into two categories on the basis of their specific gravity. Dense non-aqueous phase liquids (DNAPLs) have densities greater than water; common types of DNAPLs include timber treating oils such as creosote, transformer and insulating oils containing polychlorinated biphenyls (PCBs), and a variety of chlorinated solvents such as trichloroethene (TCE). Once released into the subsurface, these contaminants will migrate downwards through the vadose zone, into the saturated zone. As DNAPLs move downward, they accumulate and pool over permeability barriers until there is sufficient pressure to overcome the barrier. The resulting residual pools can become significant sources of long-term contamination, being advected away by groundwater flow as a dissolved phase plume.

Light non-aqueous phase liquids (LNAPLs) are less dense than water; examples of LNAPLs include kerosene, diesel and gasoline. In contrast to DNAPLs, LNAPLs will not migrate below the top of the saturated zone due to buoyancy effects, but rather accumulate above it as a free-phase contaminant, causing a depression of the capillary fringe (Parker, 1989). As the water table fluctuates, a ‘smeared zone’ is created where air, water and LNAPL are all potentially present within the pore space of the contaminated zone. The research presented in this thesis will address this category of immiscible liquid.

Subsurface contaminant sampling methods used for characterization include methods such as taking soil cores or installing monitoring wells. These techniques are generally invasive and can potentially disturb the immiscible contaminants in a way that causes further problems (e.g., creating preferential pathways for NAPL migration). In addition, by their nature, the methods provide localized information that is often difficult to extrapolate spatially across an contaminated site.

In comparison, surface geophysical techniques are very appealing as they can provide spatially extensive information about subsurface conditions in a non-invasive manner that has minimal adverse impacts. The successful application of a particular geophysical method is dependent on the contrast in its governing physical properties that occurs between the clean and contaminated regions. Given the very large difference in the electrical properties (i.e., electrical conductivity/resistivity and dielectric permittivity) between water and NAPLs, the ability of geoelectrical methods, such as electrical resistivity tomography (ERT) and ground penetrating radar (GPR), to detect NAPLs in the subsurface has been examined by number of studies. In particular, GPR has the capacity to provide high-resolution spatial imaging of the material composition of the subsurface; hence, there has been extensive investigation into the use of this technique for characterizing contaminated sites. An overview of the use of GPR for contaminant detection was given by Redman (2009).

1.1 GPR Monitoring of Subsurface LNAPL Pools

Extensive summaries of GPR theory and applications are found in the following publications: Daniels (2004), Annan (2005a, 2005b and 2009). GPR techniques are based on the propagation of electromagnetic (EM) waves through the earth. In low-loss, non-magnetic soils and sediments, EM wave propagation is essentially dependent on the dielectric properties of the subsurface.

The dielectric properties of materials are expressed in terms of dielectric permittivity ε (in Farads/meter or F/m). In geophysics, permittivity values are commonly expressed as the normalized quantity $\kappa = \varepsilon/\varepsilon_o$ called the relative permittivity where ε_o is the dielectric permittivity of a vacuum (8.8541×10^{-12} F/m). In particular, the permittivity of common NAPLs ($\kappa = 2-4$) are very low compared to the permittivity of water (κ = 80) (Lucius et al., 1992). Hence, the displacement of water by these immiscible liquids can significantly impact EM wave propagation and the GPR signature of the LNAPL affected zone.

1.1.1 Constant Offset and Common Midpoint Reflection Profiling

GPR surveys can be divided into four main types: common offset, common midpoint, common source, and common receiver. For the purpose of this thesis, the common offset and common midpoint will be discussed as they were the types employed during data collection.

Common offset surveys use a fixed spacing between the antennae; these antennae are typically orientated parallel to each other but perpendicular to the profile line. The system is

moved along the line with data collection being continuous or at a fixed interval ('step') (Figure 1.1). Stepped data collection allows better signal quality as the system is stationary during data collection. As the system moves, traces are collected at each location and plotted parallel to each other resulting in a two-dimensional reflection profile of the subsurface (Figure 1.2). Any differences in the dielectric properties of the ground result in energy being reflected back to the receiver, appearing as an event on the traces. The time between the EM wave transmission, reflection and reception is referred to as the two way traveltime and is measured in nanoseconds (ns). The common mid-point survey (CMP) uses a different method to collect reflection data where the antennae and the receiver are moved apart sequentially at a specified increment (Figure 1.3). By increasing the horizontal distance at a constant rate, the increasing two-way travel time can be used to calculate EM wave velocities, as well as the depth to a reflector. An example of a CMP radar survey is shown in Figure 1.4.

1.2 GPR Monitoring of Subsurface LNAPL Pools

There is a significant body of literature that currently exist on the application of GPR for detecting and monitoring of LNAPL in the subsurface; a list of these papers is given in Table 1.1. These papers report the findings of controlled releases into sand-packed tanks and field studies characterizing accidental releases under natural conditions. In addition, a num ber of studies reported the effects of biodegradation on the GPR signature of mature LNAPL release. Notably, the GPR monitoring performed as the first part of this overall project described by McNaughton (2011) is the first long-term GPR monitoring experiment done in actual aquifer and subjected to natural conditions over the annual cycle.

1.3 Gasoline/Ethanol Interactions

Gasoline is a significant source of groundwater contamination and its common and wide spread use throughout the world has resulted in both accidental and intentional releases. Prior to 2000, methyl tertiary butyl ether (MTBE) was added to gasoline as a fuel oxygenate; however, it was soon recognized that MTBE is a ubiquitous contaminant in both surface and ground waters. As a result of consumer complaints and health risks, the United States Environmental Protection Agency (USEPA) called for an alternate fuel oxygenate to be used. Ethanol was found to be an appealing replacement as it is a renewable biomass-based alternative which has less of a negative impact on the environment in the event of an accidental release.

North American has since embraced ethanol as a fuel additive with gasoline typically containing up to 10% ethanol by volume, and is increasingly referred to as "gasohol". The ethanol is produced and stored in large-capacity, above-ground storage tanks. During storage, the ethanol is denatured through the addition of toxic additives by at least 2% volume; typical additives (e.g., unleaded gasoline or rubber hydrocarbon solvent) are designed to render the ethanol unfit for human consumption (Rice et al., 1999). The ethanol is then distributed to blending terminals via tankers, a procedure that was identified by Rice et al. (1999) as the source of highest risk for a bulk ethanol release into the environment.

Upon release, ethanol will be primarily confined to the capillary zone due to its buoyancy, but is expected to be mobilized and dissolved with a fluctuating water table. Conversely, gasoline is almost completely immiscible with water, hence these fluids will normally exist as two distinct phases in the subsurface. While ethanol is miscible with both water and gasoline, ethanol will preferentially partition into the aqueous phase, reducing the

polarity of the aqueous phase in what is known as the "co-solvent effect" (Rice et al., 1999). This process increases the water solubility of BTEX component in the gasoline. When large amounts of ethanol are present, all three phases (i.e., ethanol, gasoline and water) can become completely miscible merging into a single phase (Rice et al., 1999).

Additionally, the presence of ethanol significantly reduces surface and interfacial tensions. This change can reduce capillary fringe thickness, as well as the volumes of the LNAPL films and residual LNAPL retained within the vadose zone (Ryan and Dhir, 1996). Finally, the reduced surface and interfacial tensions increases the mobility of gasoline (McDowell et al., 2003). This behaviour was observed in a tank experiment performed by McDowell et al. (2003) where the addition of ethanol in a pre-existing gasoline release resulted in a significant reduction in LNAPL pool height, extent and shape. This reduction was due to the ability of gasoline to now invade smaller pores, thus increasing the saturation of the gasoline within a smaller volume of the system. According to McDowell et al. (2003), this contraction of the LNAPL pool could result in less pool surface area being exposed to groundwater, lowering concentrations dissolved over a longer time frame. Similar behaviour was confirmed by Yu et al. (2009) who performed an additional tank experiment and transport modeling which showed a reduction of the LNAPL pool, and higher non-aqueous phase saturation within the contaminated zone.

Once the ethanol and BTEX are dissolved in groundwater, its fate and transport in groundwater is dependent on advection and dispersion, as well as any removal processes such as sorption and degradation. These processes both contribute to natural attenuation, and their understanding is critical for predicting the spread and extent of a dissolved-phase plume. With respect to biodegradation, it has been found that the presence of large concentrations of ethanol

in the groundwater systems will significantly affect this process. Ethanol is readily degraded under both aerobic and anaerobic conditions; thus, it will be preferentially removed relative to BTEX, consuming nutrients and electron acceptors (Mackay et al., 2006). These factors limit the natural biodegradation of BTEX, thereby resulting in a source of long term contamination.

The buoyancy, co-solvency and interfacial tension effects make characterization of sites contaminated by releases of gasoline-ethanol mixtures more difficult than sites contaminated by pure hydrocarbons. Changes in capillary fringe height due to an ethanol-induced reduction in surface tension, and mixing effects due to water table fluctuations would further complicate the determination of the rate of mass removal and LNAPL volume trapped in the vadose zone. These research questions are being examined in contaminant hydrogeology (i.e., Powers et al., 2001; McDowell and Powers, 2003; Corseuil et al., 2004; Zhang et al., 2006; Cápiro et al., 2007; and Freitas et al, 2011a,b)

1.4 Problem and Objectives

Despite the ongoing research into the characteristics and migration effects of sequential gasoline and ethanol spills in hydrogeology and geochemistry, there has been very limited research, to date, evaluating GPR as an effective tool to monitor high ethanol-content fuel releases and interactions with pre-existing gasoline (i.e., Österreicher-Cunha et al., 2004; Glaser et al., 2010; Henderson et al., 2009, Henderson et al., 2010). This previous research has been performed at the laboratory scale and has neglected the effects of co-solvency and gasoline remobilization, as well as the impact of a fluctuating water table and seasonal temperature changes on the evolution of the contaminated zones.

The research presented in this thesis was performed to address the major knowledge gap that exists in hydrogeophysics regarding the capacity of GPR to monitor the effects of ethanol released into a pre-existing gasoline contaminated zone. The starting point for this work was the controlled E10 (10% ethanol / 90% gasoline) gasoline release into the unconfined Borden aquifer conducted by McNaughton (2011), Freitas and Barker (2011) and Freitas et al., (2011); this release occurred one year earlier and was subjected to an annual cycle of in-situ conditions. In this thesis, E95 (95% ethanol / 5% gasoline) was release into the subsurface and monitored using high frequency GPR (450 MHz and 900 MHz) over the course of one year.

The specific objectives of this research are to:

- Evaluate the ability of GPR to characterize the initial remobilization of the gasoline by a subsequent ethanol release;
- Assess the capacity of GPR to monitor the evolution of the sequential gasoline-ethanol release over an annual cycle of unfrozen conditions;
- Observe and characterize the effects of the winter freeze-thaw cycle on the GPR signature of the sequential gasoline-ethanol release;

Table 1.1 - A list of previous studies concerning the use of GPR for characterizing and monitoring LNAPL releases

Setting of Release	Type of Release	Contaminant	Biodegradation	Reference
Field	Accidental	Hydrocarbons (fuels)	Yes	Sauck et al., 1998
Field	Accidental	Jet and Diesel Fuel	Yes	Werkema et al., 2003
Field	Accidental	Hydrocarbons (BTEX)	Yes	Atekwana et al., 2000
Field	Accidental	Hydrocarbons	Yes	Atekwana et al., 2010
Field	Accidental	BTEX, TMBs, Chlorinated Solvents	Yes	Bermejo et al., 1997
Field	Accidental	Hydrocarbons (fuels)	Yes	Che-Alota et al., 2009
Field	Accidental	Jet Fuel	No	Jordan et al., 2004
Field	Accidental	Gasoline	Yes	Lopes de Castro and Branco 2003
Field	Accidental	Gasoline and Diesel	No	Orlando 2002
Field	Accidental	Benzenes	Yes	Cassidy 2007
Field	Controlled	Diesel Fuel	No	Daniels et al., 1995
Field	Controlled	Gasoline	No	McNaughton, 2011
Tank	Controlled	Diesel Fuel	No	Bano et al., 2009
Tank	Controlled	Kerosene	No	DeRyck 1994
Tank	Controlled	Gasoline	No	Kim et al., 2000
Simulation	Controlled	Gasoline	No	Yu et al, 2009

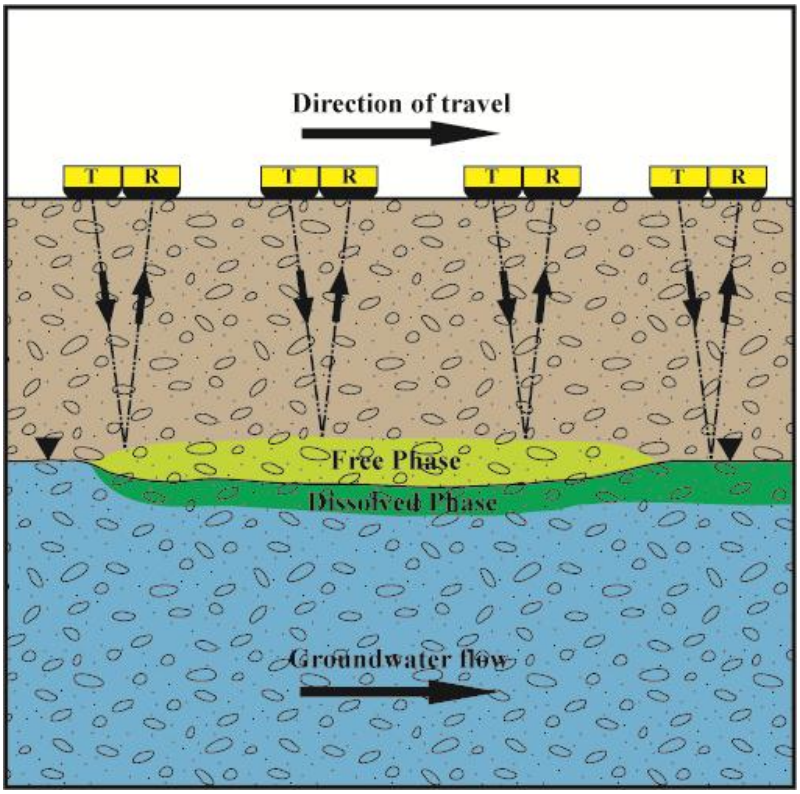

Figure 1.1 – Schematic diagram of a GPR reflection profile survey with the transmitter and receiver at a constant offset. The system is moved along the line at a fixed step size, and a sounding taken at each position.

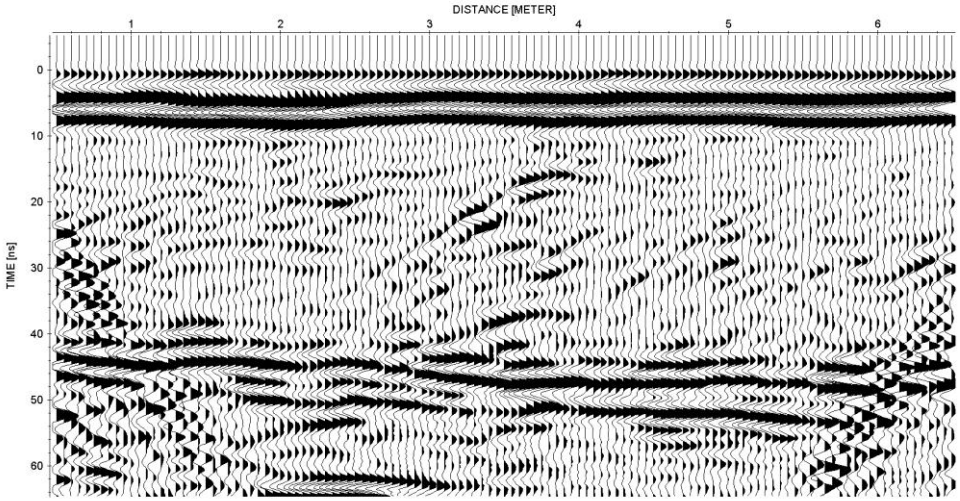

Figure 1.2 – Example of a GPR reflection profile data, showing the direct ground wave at approximately 5ns, and a stratigraphic reflection event at 40ns – 50ns.

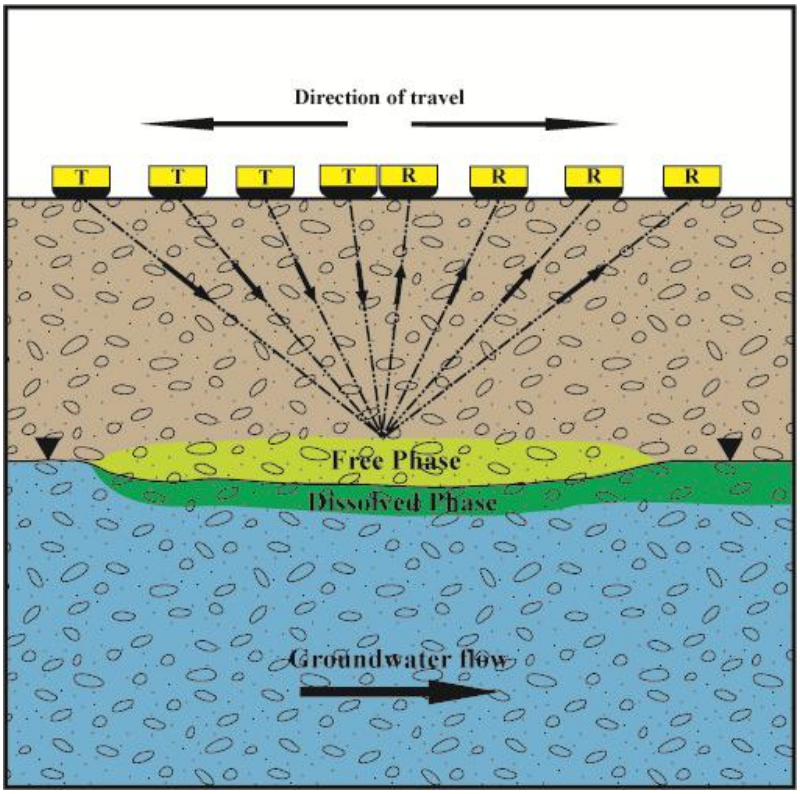

Figure 1.3 – Schematic diagram of a GPR common midpoint survey with the transmitter and receiver incrementally increasing their separation with each new position.

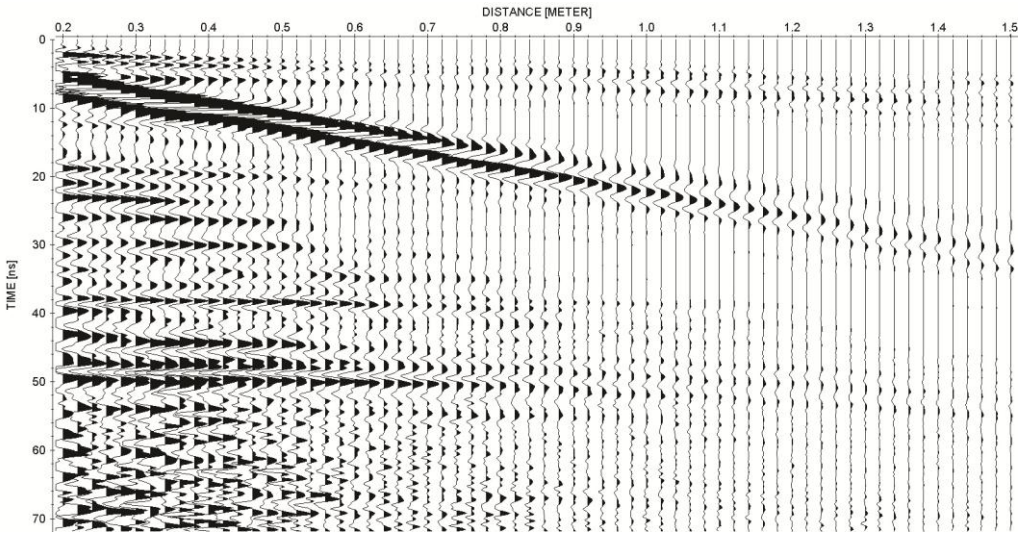

Figure 1.4 – Example GPR profile of a common midpoint survey data, showing the linear traveltime-offset dependence of direct ground wave and hyperbolic traveltime-offset dependence of stratigraphic reflection event that appear in the profile in Figure 1.2

2.0 Methodology

2.1 Site Description

This study was conducted at Canadian Forces Base (CFB) Borden located approximately 100 km North of Toronto, Ontario (Figure 2.1). Numerous internationally recognized hydrogeological studies have been performed over the past 30 years in the unconfined aquifer at this site (Sudicky and Illman, 2011). These studies have covered a wide range of hydrogeologic issues, such as contaminant transport and fate (e.g., Mackay et al., 1986; Rivett et al., 2001), geostatistics (e.g., Woodbury and Sudicky, 1991), dispersion (e.g., Freyberg, 1986; Sudicky, 1986), remediation (O'Hannesin et al., 1998; Bell et al., 2003), surface water-groundwater interaction (Abdul and Gillham, 1989 ; Jones et al., 2006) and aquifer response to pumping tests (Nwankwor et al., 1992; Bevan et al., 2005).

The unconfined Borden aquifer is a foreshore, prograding, glaciolacustrine sequence from the Pliestocene Lake Algonquin that was deposited approximately 12,000 years before present (Bolha, 1986). Sedimentary structures include horizontal to near-horizontal laminated sand beds as well as cross-laminated sand beds with dips exceeding 10 degrees. The aquifer is locally heterogeneous due to beds and lenses of fine-, medium- and coarse-grained sand (MacFarlane et al., 1983). Sudicky (1986) described the heterogeneity within the aquifer as thin laminations approximately 0.01 – 0.10 m thick and typically continuous over a scale of 2 – 5 m, resulting in spatial variability in hydraulic conductivity. The aquifer unit is approximately 7 - 8 m thick in the vicinity of the experimental site and is underlain by a clayey-silt aquitard.

Major hydrogeological characteristics that have been measuredt by previous researchers are given in Table 2.1. The water level in the Borden aquifer can vary by approximately 1.5 m annually (Conant, 1991). Given this range, the water table within the test cell can vary from approximately 1 m depth to above surface level during the annual cycle (McNaughton, 2011). Both laboratory measurements of the water content-pressure head relationship by Nwankwor (1982) and field observations with a neutron moisture probe by Bevan et al. (2005) indicated that the static moisture profile for the Borden aquifer can be generally described as having a 0.3 m thick tension-saturated zone (i.e. capillary fringe) located directly above the water table. In addition, the transition zone over which the moisture content decreases upwards to residual saturation extends an additional 0.4 m above the capillary fringe.

2.2 Test Cell Description

The release was performed in a cell, open at both ends to allow hydraulic connection with the natural groundwater flow regime. There are three adjacent cells at this site (Figure 2.2), which are constructed using sealed steel piling that is anchored into the underlying aquitard. The cell dimensions are 21 m × 7.5 m × 7 m (length × width × depth). They are oriented approximately parallel to average ground water flow direction to allow for the cells to be subject to a natural flow regime (Mocanu, 2006).

A variety of sampling instrumentation used for the geochemical analysis of the gasoline and ethanol releases were installed in the test cell; a complete description of these installations are found in Freitas (2009) and Freitas and Barker (2011). This instrumentation included

multilevel water samplers, soil gas samplers, pressure transducers and a glass well designed for a downhole camera system. The down gradient end of the test cell consisted of a reactive barrier as well as a pump-and-treat system for handling any dissolved phase contaminant.

2.3 Previous Gasoline Spill

The previous gasoline release occurred on August 21, 2008; its geophysical monitoring is described by McNaughton (2011). For this release, a 1.5 m (length) × 0.8 m (height) × 0.2 m (depth) trench was excavated and lined with a 0.5 mm plastic sheet. With the water table at 0.5 meters below ground surface (mbgs) at the time of release, the excavation trench depth resulted in complete infiltration of the gasoline directly into the tension saturated zone. The E10 mixture was prepared on site and consisted of 171 L of API gasoline standard 91-01, 9 L of MTBE (9 L) and 20 L of pure ethanol; in addition, 0.1 g/L of Oil-Red-O dye was added to make this mixture visible in soil cores. Upon complete mixing, the plastic liner was removed, permitting infiltration of the E10 mixture into the ground; the trench was covered to limit volatilization of the E10 mixture during the infiltration. Infiltration of the E10 into the soil took 5 hours; afterwards, the trench was repacked with the excavated sand.

GPR surveys were performed using a pulseEKKO 1000, manufactured by Sensors & Software Inc. in Mississauga, ON. Both the 450 MHz and 900 MHz antenna were used to acquire data. Six reflection profiles were collected at each frequency; three measuring 4.5 m in length, which were parallel to the cell walls, and three measuring 6 m in length, which were perpendicular to the cell walls. Additionally, CMP soundings were collected with both 450 and

900 MHz antenna in both parallel and perpendicular orientations at four locations. In total, each survey date consisted of 12 reflection profiles and 16 CMP soundings. Geophysical surveying lasted until June 26, 2009, resulting in 20 survey dates, including a background data set performed one day prior to the gasoline spill.

It was found that the 900 MHz antennas performed better at directly imaging the shallow contaminated zone. High-amplitude reflection events developed immediately after the release in the vicinity of the trench and expanded laterally during the initial water-table lowering. Conversely, the 450 MHz antennas allowed for the evaluation of the effects of gasoline induced velocity changes on the imaging of an underlying stratigraphic reflecting boundary (i.e., a velocity "pull-up" feature). Comparison of the 900 MHz and 450 MHz results showed that they provided consistent characterizations of the LNAPL contaminated zone extent and its temporal evolution.

2.4 Ethanol Release Methodology

September 2, 2009 (Day 0), the 200 L of E95 mixture was released into an identical trench as described above. Since that water table was located at 0.59 m bgs at the time of release, it was anticipated that release occurred above the tension saturated zone. The E95 mixture consisted of 175 L ethanol (99.9% purity, from Commercial Alcohols Inc.), and the remaining 9 L a mixture of selected compounds simulating gasoline: 82% hexane, 11% fluorobenzene, and 7% 4-bromo-fluorobenzene. This mixture was chosen to have the characteristics of the denatured ethanol that would be typically transported and stored as biofuel, yet containing different components to aid

in differentiation from the preceding gasoline release. To aid in the visual identification of the E95 release relative to the E10 release in the extracted soil cores, the ethanol mixture was dyed yellow with Fluorescein. The components were mixed in the lined trench and allowed to infiltrate into the vadose zone over approximately 1.5 hours. Once the E95 had completely infiltrated, the trench was refilled with clean sand as required by the geochemical experiment methodology to avoid the presence of gasoline above the released ethanol.

2.5 GPR Survey Design and Monitoring Strategy

The GPR profiling grid consisted of 8 reflection profile lines; the plan view of these lines is shown in Figure 2.3. Lines 2, 3 and 4 were each 6 m in length, and are positioned across the width of the cell perpendicular to groundwater flow. Lines A, B and C were 4.5 m in length running parallel to groundwater flow along the cell axis. All six of these lines were used to monitor the previous gasoline release. For the ethanol release, Lines D and E were added to provide more information about the immediate trench area, each measuring 1.8 m in length parallel to groundwater flow.

In addition to the reflection profiling, CMP soundings were done at six locations to obtain subsurface EM wave velocity information. The locations of the CMP soundings are denoted in Figure 2.3, with the maximum antenna separation being 1.5 m. Four of the CMP locations were the same as those during the earlier gasoline monitoring; however, two new locations were added in the immediate trench area.

In this study, GPR surveys were performed from July 28, 2009 through to October 01, 2010, spanning 430 days. Prior to the release of the ethanol, five GPR surveys were performed in order to establish pre-release conditions. Twenty-five GPR surveys were done after the ethanol release. The dates and the corresponding time elapsed after the ethanol release are given in Table 2.2. During each GPR survey date, all eight reflection profiles were acquired using two different sets of frequency antennas (i.e., 450 and 900 MHz). CMP sounding were also collected with perpendicular antennae orientation at all six locations with both antenna sets. In addition, CMP soundings collected with parallel antennae orientation were collected at all six locations with the 900 MHZ antenna set. This acquisition program resulted in a total of 34 GPR profile lines and CMP soundings being collected during each GPR survey date.

2.6 GPR Equipment

The GPR system used to collect data was a pulseEKKO 1000 manufactured by Sensors & Software Inc. in Mississauga, ON. The pulseEKKO 1000 is equipped with shielded antennae that permit applications in enclosed environments (i.e., antenna design focuses energy into the ground, thereby limiting above ground reflections that may interfere with subsurface events). There are a number of acquisition parameters that need to be selected for GPR acquisition; Table 2.3 lists the values of these parameters used in this project. The time window is the overall time period, in nanoseconds (ns), for which the unit records arriving events at the receiving antenna; this window must be long enough to record the arrival of the desired events. The sampling interval is the time increment in picoseconds (ps) between discrete signal measurements during recording; its value must consider acquisition effort and the potential of temporal aliasing. The

stack is the number of times each trace is superimposed to enhance the signal to noise ratio of the GPR data. Antenna separation, in metres, is a constant offset distance between the antennas during the reflection profiling. The pulseEKKO 1000 has a bracket system to maintain a recommended offset; these brackets were used in this project. The step size is the spatial increment the antennas are moved for each trace. For reflection profiling, the step size is the distance the antenna array is moved between samples, while step size for the CMP sounding is the incremental increase in the antenna offset distance as traces are collected. The choice of the step size must consider potential spatial aliasing effects as well as acquisition efficiency.

2.7 GPR Data Processing

Following data acquisition in the field, GPR data requires processing to enhance subsurface reflection events and suppress random noise. Initially, the data was downloaded from the data logger to a desktop computer using WINPXFER (Sensors & Software Inc.). Subsequently, the data was imported into EkkoView Deluxe v1.3 (Sensors & Software Inc.) where each line was renamed to include the date, survey number, and a unique identifier of the profile line and survey type. The data was then inspected to ensure the correct survey parameters (i.e., start and stop positions, number of traces and step size) were in the header files and that there were no blank traces present in each data set. In the very infrequent cases when blank traces were found, the EkkoView Deluxe software was utilized to replace these blanks by interpolating between adjacent traces.

Once the data quality had been verified, zero time adjustments were made to both the 450 and 900 MHz reflection profile data. This procedure was done to ensure that the first break from the GPR reflection was positioned at 0 ns, thereby giving the profiles a consistent start time. This adjustment was accomplished using the Repick Timezero tool in EkkoView Deluxe software with the default ± 5% amplitude threshold value. Next, the overall time window was reduced to -5 ns to 40 ns for 900 MHz profiles and -5 ns to 65 ns for 450 MHz profiles. This shortening of the time window reduced the amount excess time data that did not contain useful information about the subsurface, and produced a consistent time range for comparison of individual profiles for each antenna frequency.

The remainder of the post-acquisition data processing of the reflection profiles was performed in the ReflexW version 5.5 software package developed by Sandmeier Software. The following five processing steps were performed in this order: dewow, bandpass filtering, gain function, running average spatial filtering and mean filter. The parameter values selected for each processing step are summarized in Table 2.4. Two different objectives guided the post-acquisition processing performed on the reflection profiles. The 900 MHz profiles were processed to enhance the reflection events from the shallow LNAPL contaminated zone. In contrast, the 450 MHz profiles were processed to improve the imaging of the reflection event from a deeper continuous stratigraphic boundary underlying the entire test cell. These two contrasting processing objectives combined with the differing antenna frequencies resulted in two sets of processing parameter values.

2.8 GPR 450 MHz Reflection Data Time-picking

The 450 MHz data are used to evaluate the change in traveltime for the reflection from a laterally continuous stratigraphic interface underlying the test cell. Similar to the gasoline, the dielectric permittivity of ethanol ($\kappa \sim 25$) is lower than that of water ($\kappa \sim 80$). Hence, the displacement of water by gasoline and/or ethanol will result in increased EM wave velocity within the contaminated zone, over the reflecting interface. In turn, this change decreases traveltime of the stratigraphic reflection event and produces an apparent pull-up of the reflector directly below the contaminated zone. Figure 2.4 show an example of this velocity pull-up effect.

By determining the change in traveltime relative to the background data collected prior to the ethanol release (Sept 1, 2009), we can infer the presence of the contaminated zone. The stratigraphic reflection at approximately 45 ns shown in Figure 2.4 was easily identified on all of the reflection profiles obtained from the cell. The traveltime to this reflection was determined using the event picking routine in the ReflexW package. This traveltime data was differenced with corresponding traveltime data obtained from the pre-release background survey obtained on Day -1 (Sept 01, 2011). Because the stratigraphic interface is fixed in location, these changes in traveltime indicate velocity changes in the overlying subsurface.

However, these traveltime measurements are complicated by the fluctuating water table and moisture profile. These changes in water content would be expected to add a unique bulk shift to the traveltime of the stratigraphic reflection across the entire survey for a given date. In an attempt to compensate for these water table fluctuation effects on the traveltime measurements, the 450 MHz reflection profiling along Line 4 were used to estimate the bulk shift. This process was felt to be reasonable given the lack of release induced impact seen along

this down-gradient line during and after the gasoline release (McNaughton, 2011) and observed in this experiment prior to the onset of winter conditions.

Figure 2.5 shows the comparison of the shallow reflection event imaged by the 900 MHz profiles, the reflector pull-up on the 450 MHz profile, and changes in 450 MHz traveltime for Line 3. It can be seen that there is a good correlation of the 900 MHz high-reflectivity events and the stratigraphic pull-up effect as plotted with the 450 MHz reflector. By applying this technique to all six lines and using the software package Surfer to interpolate between lines, various plan view maps were created to visualize the spatial extent and magnitude of the traveltime variations. These results are presented in Section 3.

Table 2.1 - Estimates of Borden aquifer properties	
Average groundwater velocity	0.09 m / day [A]
Horizontal Hydraulic Gradient	
Magnitude range	0.0035-0.0065[AB]
Magnitude annual mean	0.0043[B]
Direction annual mean	N 21° E[C]
Hydraulic Conductivity	
Range	$5x10^{-7} – 2x10^{-4}$ m/s[B]
Geometric mean	$7.2x10^{-5}$ m/s[B]
Standard deviation of natural log	0.62[B]
Porosity	
Mean	0.33[A]
Coefficient of variation	0.05[A]
[A] Mackay et al, 1986 [B] Sudicky, 1986 [C] Martin, 2004	

Table 2.2 – Dates/time elapsed of GPR surveys

Background Dates			Monitoring Dates		
Data	**Date**	**Day**	**Data**	**Date**	**Day**
M20	28-Jul-09	-36	E01	2-Sep-09	0
M21	18-Aug-09	-15	E02	3-Sep-09	1
M22	25-Aug-09	-8	E03	4-Sep-09	2
M23	31-Aug-09	-2	E04	5-Sep-09	3
M24	1-Sep-09	-1	E05	6-Sep-09	4
			E06	7-Sep-09	5
			E07	9-Sep-09	7
			E08	11-Sep-09	9
			E09	14-Sep-09	12
			E10	18-Sep-09	16
			E11	23-Sep-09	21
			E12	30-Sep-09	28
			E13	7-Oct-09	35
			E14	21-Oct-09	49
			E15	13-Nov-09	72
			E16	14-Dec-09	103
			E17	11-Jan-10	131
			E18	26-Jan-10	146
			E19	2-Mar-10	181
			E20	3-Apr-10	213
			E21	30-Apr-10	240
			E22	23-Jun-10	294
			E23	6-Aug-10	338
			E24	9-Sep-10	372
			E25	1-Oct-10	394

Table 2.3 – Survey parameters used during the collection of the GPR data		
Parameter	**900 MHz Antenna**	**450 MHz Antenna**
Time Window	50 ns	80 ns
Sampling Interval	100 ps	200 ps
Stack	64	64
Antenna Separation	0.17 m	0.25 m
Profile Survey Step-size	0.02 m	0.05 m
CMP Survey Step-size	0.02 m	0.02 m

Table 2.4 – GPR processing steps and parameters used in ReflexW		
Processing Filter	**900 MHz Parameters**	**450 MHz Parameters**
Subtract-mean (dewow) (timewindow)	1.11 ns	3 ns
Band Pass Frequency (Lower cutoff/Lower plateau/Upper plateau/Upper cutoff)	100/200/1600/2000	50/100/1250/1550
Gain Function (Start time/Linear gain/Exponent/max gain)	0 ns/0.8/10/100	0 ns/0.045/10/500
Running Average (Average traces/Start time/End time)	3/-5 ns/40 ns	3/-5 ns/65 ns
Mean Filter (Mean range)	5	8

Figure 2.1 – Location of Canadian Forces Base Borden, Ontario Canada.

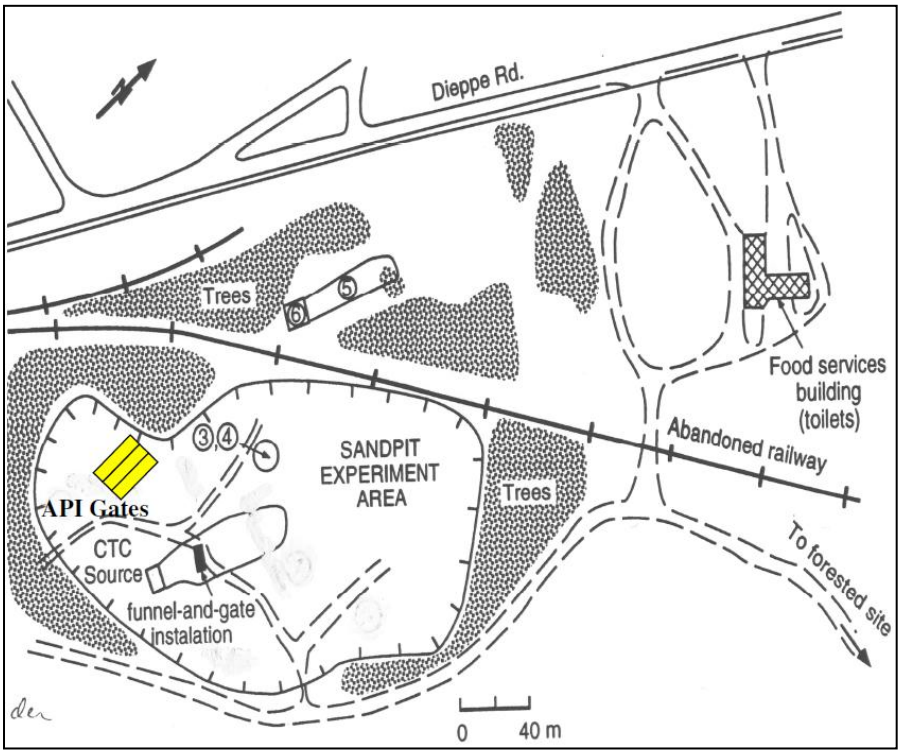

Figure 2.2 - Location and orientation of the three gates, shown in yellow, within the sand pit (Mocanu, 2007)

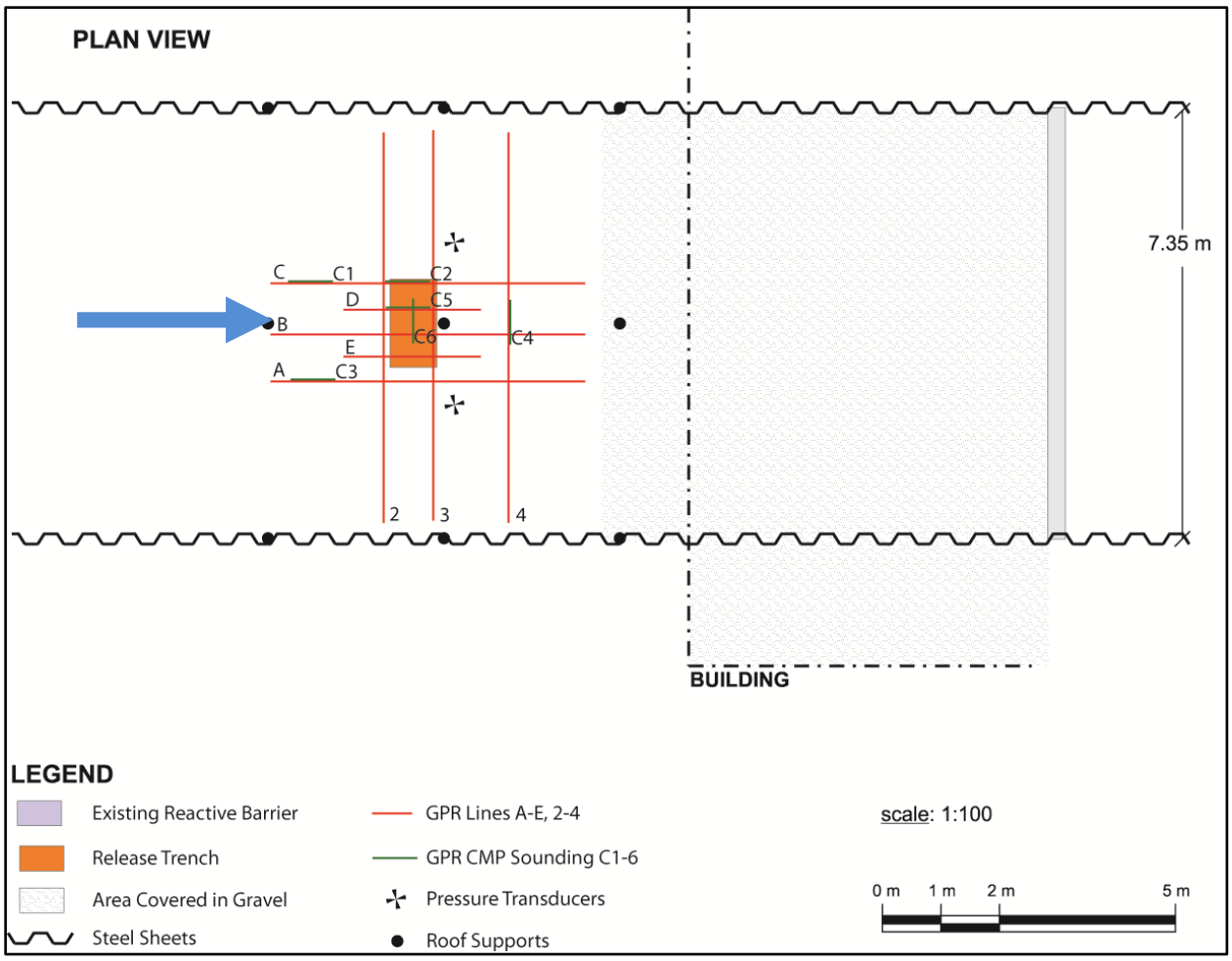

Figure 2.3 – Plan view of the test cell with radar reflection profile lines and CMP sounding locations shown in relation to the release trench and cell walls

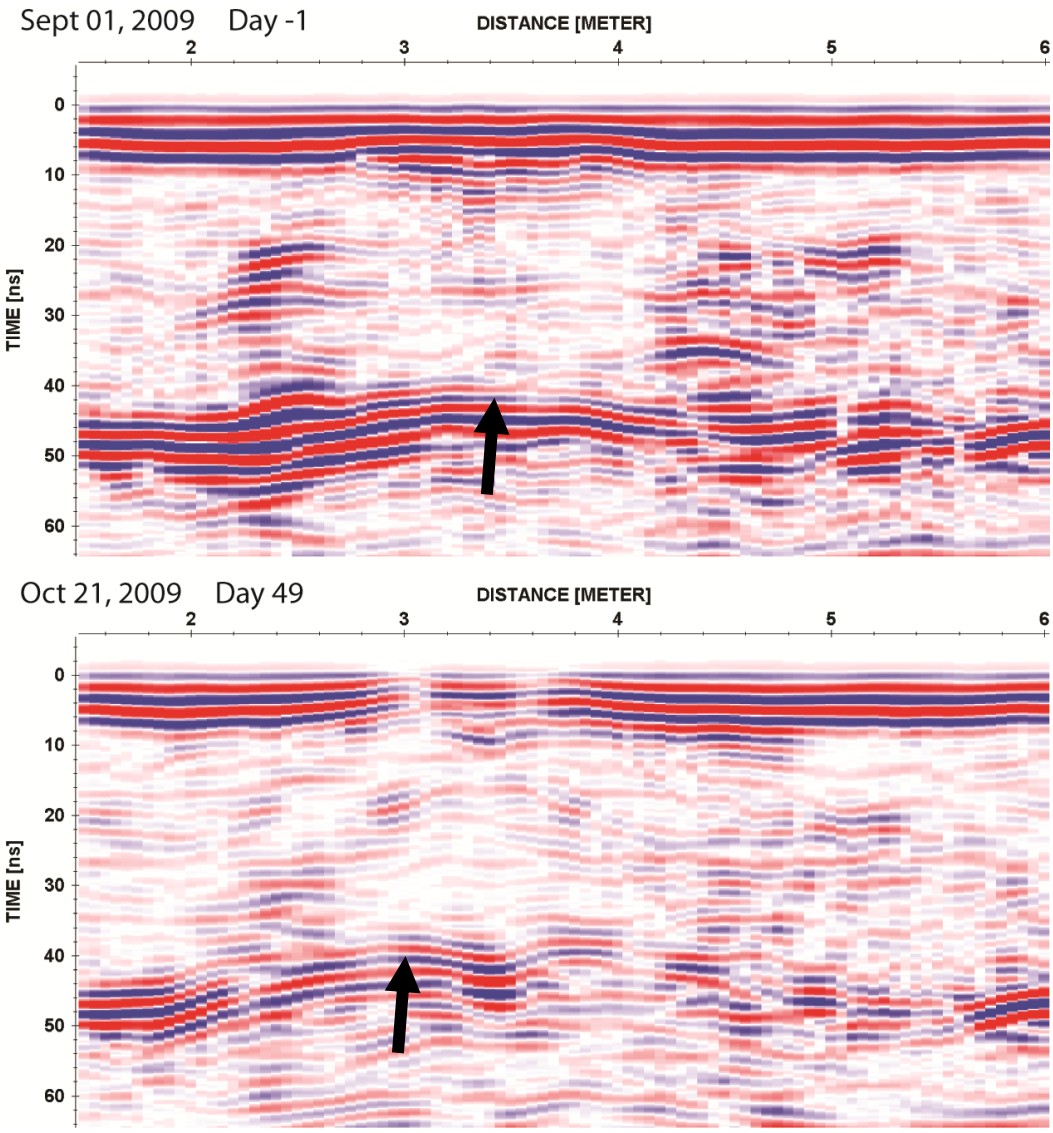

Figure 2.4 - Example of 450 MHz reflection profile along Line 3, showing the velocity pull-up of the stratigraphic reflection at approximately 45 ns (Arrow). Both pre-and post-release profiles are shown for comparison.

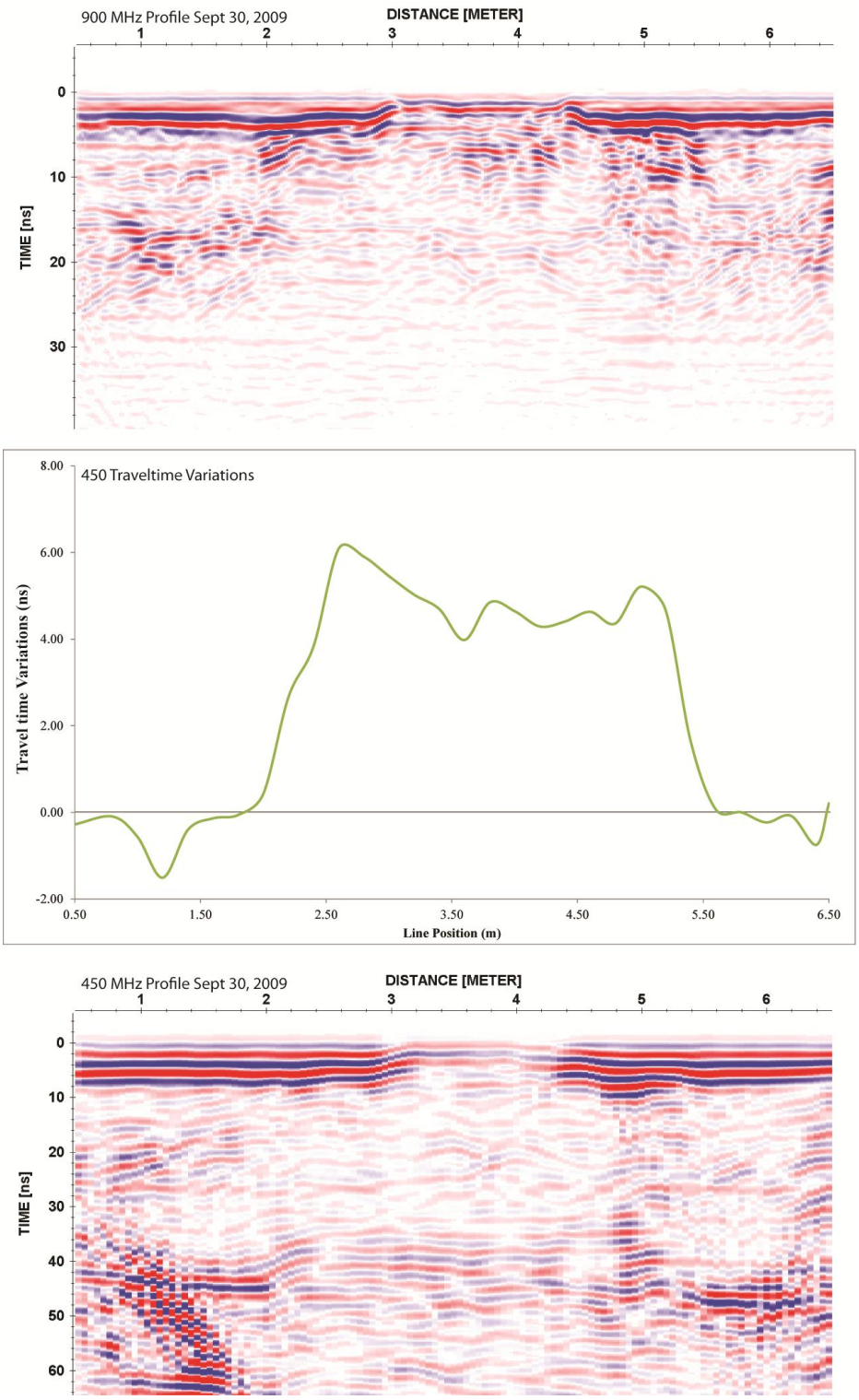

Figure 2.5 – A correlation of the shallow reflectivity event on the 900 MHz and 450 MHz traveltime variations on Line 3. For the 450 MHz data, both the measured traveltime change and the corresponding reflection profile are shown. Sept 30, 2009 (Day 28)

3.0 GPR Data Analysis and Interpretation

This section examines the evolution of the contaminated zone as observed in the GPR reflection profiling data sets acquired during this experiment. The temporal evolution of the ethanol-contaminated zone was monitored for 394 days after the release. This extended monitoring period permitted observation of remobilization processes, as well as the effects of seasonal variation in subsurface conditions on the contaminated zone. In this study, seasonal soil conditions included the development of a frozen surface layer during the winter period and water table dynamics associated with groundwater recharge events.

Due to differences in resolution and depth of penetration, the GPR results have been divided into two sections based on antennae frequency (i.e., 900 MHz profiling in Section 3.1 and 450 MHz profiling in Section 3.2). While the 900 MHz profiling provided better imaging of the shallow contaminated zone, the 450 MHz profiling had better depth of investigation, permitting the analysis of a velocity pull-up effect on a stratigraphic reflection from underlying interfaces. In addition, soil cores and an impedance depth survey were collected during this experiment for comparison with the GPR; these results are presented in Section 3.3.

An important element of this experiment was the impact of the varying water table. Figure 3.1 shows the water table measurements obtained from pressure transducers located in a monitoring well in the test cell with the GPR monitoring dates superimposed. The summer of 2009 is characterized by a generally declining water table that is punctuated by precipitation events that resulted in substantial water table rises. This behaviour can be seen on three

occasions prior to the release on Sept 02, 2009, with the most dramatic rise occurring on Aug 10, 2009 where the water table rose to 0.21 mbgs. The resulting water table rises due to these precipitation events elevated the saturated zone to the level of the release trench, thus the start of this experiment was delayed until a suitable lower water table level was obtained. These conditions were achieved in early September when the water table lowered to 0.62 mbgs, at which point the ethanol was released into the subsurface.

Throughout the experimental monitoring period, the test cell was subject to naturally occurring seasonal change in both temperature and groundwater flow conditions. The main features of these conditions are as follows. During the remainder of September after the ethanol release, the water table was characterized by a continued decline to a maximum depth of 0.75 mbgs. In early October, the water table rose approximately 10 cm and fluctuated between 0.65 to 0.70 mbgs level through the October and November period.

A consistent water table decline to a depth of 0.92 mbgs was observed over the December-February period. During this period, frozen conditions in the near-surface developed at the test site. These frozen conditions drastically altered the GPR response and provided a unique data set spanning January to early March. The spring thaw in the middle of March produced a drastic increase in the water table, from 0.92 mbgs on March 5th to 0.41 mbgs on March 14th. The water table fluctuated about this higher level through the spring and underwent a progressive decline during the following summer and early fall of 2010. These water level data are punctuated by shorter duration peaks that are most likely due to individual precipitation events.

3.1 900 MHz Profiling Results

Of the eight reflection profile lines collected, the results presented in this chapter will focus on 900 MHz reflection profiling data from Lines B, 3 and 4. Line B is oriented along the axis of test cell and crosses the center of the release trench, while Line 3 is oriented perpendicular to the cell and is located along the down gradient edge of the release trench. Both of these lines clearly show the effects of the ethanol release on the GPR response. In comparison, Line 4 which is located approximately 1.5 m down-gradient of the release trench is unique in that it is the only GPR line not impacted by original gasoline monitored by McNaughton (2011) or the initial expansion phase of the ethanol release of this study.

3.1.1 Pre–release Distribution of Gasoline Residuals

Prior to the ethanol release on September 2, 2009, five background GPR surveys were performed on Days -36, -15, -8, -2 and -1 to characterize the pre-existing geophysical signature of the emplaced gasoline from the initial release in August 2008. These background reflection profiles for Line 3 given in Figure 3.2 show a series of multiple high-amplitude reflection events directly below the release trench (i.e., between positions 3.00 m to 4.35m). Likewise, background profiles from Line B shown in Figure 3.3 display similar reflection events beneath the trench location between 2.80 m to 3.70 m. These multiple reflections are believed to represent the approximate position of the pre-established gasoline residual zone. In the previous gasoline experiment by McNaughton (2011), it was concluded that the gasoline pool remained stationary, with the majority of the mass contained within the area of and below the initial release trench. This hypothesis is supported by the reflection profiles collected along Line 4 (Figure 3.4) which

show no anomalous reflection events, and thus no evidence of gasoline residual from the initial gasoline release. This interpretation is consistent with background GPR reflection data collected prior to the ethanol release.

3.1.2 Ethanol Release and Initial Remobilization of the Gasoline

Since the release trench had to be packed with clean sand after the ethanol release to avoid the presence of gasoline above the ethanol phase, there was an inherent contrast in electrical properties between the trench fill and the surrounding contaminated soil. This contrast affected the nature of the direct ground wave (i.e., the event that travels along the surface between the antennas). These effects of this can be seen readily in first-arrival events of the post-release GPR profiles for the position located on the trench; these positions are denoted by green lines in the figures. However, it appears that this fill had minimal impact on the imaging of the underlying contaminated zone and the stratigraphic interfaces.

Immediately after the release on Sept 2, 2009, significant changes were observed on the 900 MHz reflection profiles in the gasoline-contaminated zone below the trench. These changes can be seen in the profiling done along Lines 3 and B (Figures 3.5 and 3.6, respectively), and are absent along Line 4 (Figure 4.7). The high-amplitude events located between 5-12 ns below the trench that were inferred due to the gasoline residuals in the pre-release imaging appear to shift downwards and somewhat contract in lateral extent from Day 0 to 7. This response appears to be consistent with the capillary fringe depression and gasoline redistribution observed in laboratory test cells (Freitas, 2009)

After this time, the amplitude of these events below the trench significantly dissipates. While there is still a limited zone of substantial reflectivity below the trench on Line B (Figure 3.6) through Day 49, the reflectivity below the trench along Line 3 (Figure 3.5) is almost completely reduced. It is possible that this behaviour is a manifestation of the co-solvency effects of ethanol on gasoline (e.g. McDowell et al., 2003). This phenomenon would be expected to reduce the contrast in electrical properties across interfaces in the contaminated zone.

In addition, high-amplitude shallow reflection events were observed along the trench periphery which progressively moved laterally away from the trench. This lateral movement was observed on the reflection profiling through Day 28 which corresponded with the lowest water table depth observed in the Fall of 2009 after the release. At this point, these events reached a maximum extent of 1.80 m to 5.60 m along Line 3 (Figure 3.5) and 1.95 m – 4.85 m along Line B (Figure 3.6).

These laterally expanding events also occurred on the other survey lines where the initial gasoline release was imaged by GPR profiling (i.e., Lines 2 and C), seen in Figure 3.8. In all cases, the maximum lateral extent of these events is greater than the similar high-reflectivity feature observed after the initial 2008 gasoline release reported in McNaughton (2011). In addition, these events were observed to develop on Line A (Figure 3.8), McNaughton (2011) did not report the appearance of such an event during monitoring of the gasoline migration. After the early October water table rise, these events cease their lateral movement on the GPR reflection profiles and exhibit a progressive decrease in reflectivity.

In contrast to these results, the reflection profiles acquired along Line 4 (Figure 3.7) shows no significant changes in GPR response during this initial monitoring period. These

results are analogous to that reported by McNaughton (2011) for the initial gasoline release. In both cases, the lack of change in the GPR images is inferred to indicated that immiscible phase displacement did not occur along Line 4, which is further down gradient from the trench.

3.1.3 Long-Term Evolution of the Ethanol Release

Figures 3.9-3.11 show selected reflection profiles along Lines 3, B and 4, respectively, during the later portion of the geophysical monitoring period from Day 51 to the end of the experiment on Day 394. During this period, changes in the geophysical response appear to be strongly influenced by watertable variations and the occurrence of the seasonal freeze-thaw cycle.

For the remainder of the Fall of 2009, the shallow lateral reflection events on the GPR images obtained along Lines 3 and B continue their progressive decrease in reflectivity. The characteristics of the reflection profiles change radically with the development of frozen soil conditions. These conditions were first encountered on Day 103 (December 14, 2009). On this date, the diminished amplitude of direct ground wave events (i.e., the first arrivals) can be observed at the ends of profile Lines 3 and B; this direct ground wave behaviour is indicative of the presence of a thin frozen surface layer (Steelman and Endres, 2009). The contrasting higher-amplitude direct ground wave event over the location of the shallow lateral events that developed after the release indicate lateral variations in the development of very shallow ground frost. Similar direct ground wave features were also observed on Day 103 along Line 4 (Figure 3.11).

During the course of the winter period (i.e., January 11, 2010 (Day 131), January 26, 2010 (Day 146), and March 02, 2010 (Day 181)), a generally strong and laterally extensive reflection event was observed to form that progressively migrated downward on the profile in

Figures 3.9-3.11. The characteristics of this event are consistent with the reflections from the base of the frozen soil zone (Steelman et al. 2010). This event exhibits delayed traveltimes beneath a zone of differing direct ground wave characteristics, which indicate lateral variation in near surface conditions. In addition, the frost-base event initially varied in amplitude laterally such that it appeared to be discontinuous from 4.2 m – 5.2 m, along Line 3 on Days 131 and 146. This discontinuity was absent on Day 181 (March 02, 2010), during which the frost-base event appeared to have migrated deeper into the subsurface. This observation is further discussed in Section 3.3.2.

The changes in the direct ground wave characteristics and delayed frost-base traveltimes appear to be due to lateral variations in the freezing process. Their location on Lines 3 and B coincide with the shallow lateral high reflectivity events that developed after the release but have somewhat greater lateral extent. For example, Line 3 shows the post release event on Day 49 which covers the interval 1.9 m – 5.6 m, in comparison, the freezing zone anomaly seen on Day 146 extends from 1.6 m – 5.9 m. Further, these freezing zone anomalies were also observed on Days 131-181 along Line 4 (Figure 3.11). This appearance of a depth depressed freezing process anomaly was unexpected since reflection profiling done during earlier unfrozen conditions gave no indication that Line 4 had been impacted by the ethanol release. If it is assumed that the frost zone base is located at a relatively constant depth on any particular survey date, then the delayed traveltimes would be indicative of unfrozen conditions. These conditions were confirmed through the use of a physical impedance measurement, and are further discussed in Section 3.3.2.

By early April, the snow had essentially melted and the ground had thawed. This release of stored water resulted in a sharp increase in the water table (i.e, an increase from 0.92 mbgs to 0.41 mbgs) as shown in Figure 3.1. With the capillary fringe extending 0.3 m above the water

table, it would be expected that saturated conditions would have almost reached the surface. The water table fluctuated about this shallow level through to the early summer period and is captured by the profiling done on Days 240-294. Throughout this period, the reflection profiles exhibit significantly decreased reflectivity, providing little, if any indication of the contaminated zone.

The nature of the reflection profiles radically evolved as the water table underwent a progressive lowering during the remainder of the monitoring period (i.e., Fall of 2010). On Days 338-394 in Figures 3.9-3.11, it can be seen that extensive increases in reflectivity developed on Line 3, B and 4, respectively. The lateral extent of these events corresponds with the locations of the frozen soil anomalies which are greater in extent than that of those immediate post-release events imaged on Day 28. The presence of the high-amplitude events on days 372 and 394 along Line 4 (Figure 3.11) is another indication that the impact of the ethanol release had significantly moved in the down-gradient direction during the later portion of the monitoring period.

3.2 450 MHz Reflection Profiling Results

Selected 450 MHz reflection profiles for Lines 3, B, and 4 are displayed in Figures 3.12, 3.13, and 3.14, respectively; the dates shown are Days 0, 5, 28, 49, 338 and 394, as well as the day prior to the spill (Day -1) as an example of the background profile. The direct ground wave event (i.e., first arrival) and the continuous stratigraphic reflection event at 45 – 50 ns can be consistently seen on the 450 MHz reflection profiles throughout the monitoring period. While similar features are visible in the shallow zone directly impacted by the ethanol release (i.e., down to 15 ns) on the 450 MHz reflection profiles, they are less well resolved due to the lower

frequency resolution and are also partially obscured by the superposition of the direct air-ground wave arrival.

The traveltime of the deeper stratigraphic reflection undergoes a general decrease after the ethanol release when compared with the pre-release profiling. Since this interface has a fixed depth, this traveltime decrease, commonly referred to as a "velocity pull-up", of the stratigraphic reflection is due to an increase in EM wave velocity of the overlying material. This velocity increase would result from the displacement of lower velocity pore water (~0.033 m/ns) by higher velocity fluids such as air (~0.30 m/ns), ethanol (~0.067 m/ns) or gasoline (~0.19 m/ns). Velocity pull-up features have been documented by previous Borden DNAPL (Brewster and Annan, 1994) and LNAPL (DeRyck 1994) experiments. In addition, comparison of the 900 MHz and 450 MHz profiling results clearly shows that there is very good correlation between the locations of the velocity pull-up and the shallow reflection event. Hence, it is reasonable to assume that the velocity pull-up can be used to infer the extent of the contaminated zone.

In Figures 3.12 and 3.13, the velocity pull-up is seen on profiling from Lines 3 and B, respectively. Immediately after the release (Days 0 and 5), scattering directly below the release trench partially obscures the deeper stratigraphic event. This scattering progressively diminishes and the pull-up is clearly visible on the profiles for Days 28 and 49. Analogous to the 900 MHz profiling results for the following spring and summer period, there is little, if any, evidence of the pull-up during the seasonal water table high in June (Day 338), yet it reappears once the water table had fallen during the summer period (Day 394). For the profiling along Line 4 (Figure 3.14), it can be seen that there is no apparent pull-up in the early period after the release (Days 0-49). However, there are traveltime variations below the location of the emergent reflection events observed on the 900 MHz profiles after the water table lowered on Day 394.

This velocity pull-up is further evidence that the contaminated zone had moved down gradient to Line 4.

To quantify the traveltime change of the continuous stratigraphic reflector found between 40-50 ns on the 450 MHz data, its traveltime at each sounding position along the profile line was differenced with the corresponding value from the background data set collected on Day -1. A positive traveltime difference indicates higher velocities relative to background conditions, and thus the presence of a higher EM velocity material overlying the interface. Conversely, a negative traveltime difference would indicate a slower EM wave velocity conditions relative to background.

An example of these traveltime differences for Line 3, are shown in Figure 3.15 for the dates corresponding to the profiles given in Figure 3.12. It can be seen that both the magnitude and lateral extent of the traveltime pull-up increases from the date of ethanol release until Day 28. This response is maintained through Day 49. During spring high water table conditions following the major seasonal recharge event, the velocity pull-up had essentially disappeared (Day 338). Once the water table undergoes the season summer drop, the traveltime pull-up reappeared (Day 394).

To investigate the spatial variability of the traveltime differences for the deep stratigraphic reflection event, planview diagrams were created from the 450 MHz traveltime differences determined from each 450 MHz profile relative to the corresponding background data from Day -1. The traveltime difference measurements from six lines (Lines A-C and 2-4) were imported into Surfer version 9 (Golden Software Inc.), and contoured over the area of the

test cell using the kriging interpolation method. The planview traveltime differences shown in Figures 3.16-3.18 cover the entire monitoring period including the multiple pre-release surveys.

The planview map for the cell in Figure 3.16 shows the traveltime differences in the pre-release surveys prior to the chosen background reference on Day -1. The local variations in traveltime observed during this pre-release period are generally on the order of 1 – 2 ns which are relatively small compared to the release inducted changes described below and are pervasive over the survey area. A possible source for these variations is localized water content variation in the near surface associated with soil heterogeneity.

Once the ethanol was release on Day 0, there was an immediate effect on the traveltime planviews, which is clearly illustrated in Figure 3.17. These traveltime differences increases in magnitude and spatial extent during the initial phase covering the remobilization of the gasoline. Planviews for Days 0 through 4 show preferential accumulation along the up-gradient side of the trench, whereas planviews for Days 5 to 12 show the pull-up occurring over the entire release trench area and into the surrounding region. The greatest magnitude of traveltime difference was measured on Day 21 and gradually decreases afterwards through Day 49. The spatial extent of the pull-up continues to progressively increase through Day 49. At this point in the post-release monitoring, the movement of the traveltime difference appears to be roughly equivalent in both the up-and down-gradient directions relative to the release trench.

The longer term evolution of the traveltime differences during unfrozen conditions in response to the changing water table levels are shown in Figure 3.18. The spatial extent of the pull-up appears to stop expanding by Day 72 and is relatively unchanged on Day 103 prior to the onset of frozen winter conditions. However, the magnitude of the traveltime variation does

appear to continue its progressive decrease over this time. Days 213-394 show the traveltime difference changes during the spring-early summer high water table conditions and its subsequent progressive drop through the end of the monitoring period. During the water table high stand (Days 213-294), there is little, if any indication of traveltime differences consistent with the earlier monitoring data on Day 103. As the water table lowers (Days 338-394), the traveltime differences progressively re-emerge, though the magnitudes are well below the pre-winter values. Further, its spatial extent is much larger, particularly in the down gradient direction.

It should be noted that the traveltime difference measurements for the frozen conditions are not included in this section. Since the EM wave velocity of ice (i.e., $v \approx 0.17$ m/ns), is much higher than water, the basis for the velocity contrast between the ethanol-contaminated zones and the unimpact regions is probably no longer valid during these condition. The traveltime difference data from this period will require a level of analysis beyond the scope of this study.

3.3 Comparison of GPR Profiling Results with Other Data

While it is quite apparent from the reflection profiling results presented in the previous chapter that GPR strongly responds to the evolving subsurface conditions, it is important to compare these geophysical responses to other measurements and observations obtained during this experiment. For this experiment, two sets of independent data were specifically acquired to further our understanding of the GPR results. The first set is a series of soil cores taken during the initial evolution of the contaminated zone that was observed after the ethanol release. The

second set of data being the validation of the depressed frozen zone by physical impedance probing. These auxiliary site investigations are discussed below.

3.3.1 Soil Core Comparison with GPR

On October 30, 2009 (Day 58), four soil cores were taken along Line 2 to compare the gasoline/ethanol contaminated zone inferred from GPR reflection profiling to geochemically sampled values. The cores were collected at the 1.80 m, 2.40 m, 2.85 m, and 3.70 m positions (i.e., Cores 1 to 4, respectively) along the survey line. The location of these cores were intendedto give a cross-sectional view of the contaminated zone perpendicular to the hydraulic gradient, outward from the axis of the release trench. These cores were sampled at 3 cm – 5 cm intervals to a total depth of 72 cm. The sampling procedure and geochemical interpretation are described in Freitas (2009). The results are presented in Figure 3.19 with the GPR profile data collected 9 days earlier on Oct 21, 2009 (Day 49).

At the time of coring, the water table was located at 0.585 m depth below the surface. The analysis of Core 1 shows the absence of both gasoline and ethanol, with the possible exception of the very minor amounts of ethanol at the surface. In addition, there appears to be a fully developed capillary fringe above the watertable at this location.

In contrast, Cores 2 through 4 all contain significant amounts of gasoline and ethanol that extend from the surface to depths of at least 0.40 meters. Significantly reduced water saturations were also found at all three locations. Qualitatively, these cores show an overall increase in total gasoline and ethanol mass near the trench axis. In addition, it can be seen that the amount of gasoline, and to a lesser extent ethanol, below the water table increases toward the trench axis.

A shallow reflection event of the type described in Section 3.1.2 can be seen on the 900 MHz reflection profile in Figure 3.20 extending from 1.6 m to 5.8 m along Line 2 on Day 49. However, the nature of this event changes at its periphery from relatively horizontal (i.e., 2.0-5.5 m) to having significant apparent dips (i.e., 1.6-2.0 m and 5.5-5.8 m). The lack of ethanol and gasoline in Core 1 indicates that these dipping events are likely diffractions. Diffraction events are scattered signal that are generated by sharp lateral boundary between the clean and ethanol/gasoline contaminated zone and distort the imaging of this boundary using surface reflection profiling. This result demonstrates that determination of the lateral extent of the contaminated zone from the 900 MHz reflection profiling needs to consider the effects of potential diffraction events.

The velocity pull-up determined using the deeper stratigraphic event found on the 450 MHz reflection profiles extends from 2.0 m to 5.6 m along Line 2 on Day 49. This lateral extent of the pull-up is consistent with the location of the contaminated zone as defined by these soil cores. In addition, the variation in the ethanol and gasoline contents seen in the cores appears to be qualitatively related to the 450 MHz velocity pull-up seen in Figure 3.18. In this figure, the traveltime difference increases with proximity to the trench, indicating higher concentrations of gasoline and ethanol contained within the unsaturated zone.

3.3.2 Physical Impedance Probing Comparison with GPR

Physical impedance probing was performed to establish the top of the wintertime frozen zone; this was conducted on two days (i.e., January 26, 2010 and March 08, 2010). This method, which is similar to that used to determine active zone thickness in permafrost (e.g., Arcone and Delaney, 2003), was performed using a steel rod inserted by hand into the ground until rejection

occurred. It is assumed that the rejection happens at the top of the frozen zone. Depth to the frozen zone was recorded upon removal of the steel rod, and repeated along each of the lines at a 10 - 20 cm sampling interval.

Comparison of the GPR 900 MHz profiles and the recorded depth to the frost zone found very good correlation between these data sets. This correlation is seen in Figures 3.21 and 3.22 where the depth data closely follows the form of the frost table top as imaged by the 900 MHz reflection profile along Line 3. The apparent window observed in the GPR was coincident with the absence of freeze-thaw interface.

Figure 3.33 shows January planviews based on the interpolated probing rod depths and measured traveltimes to the frozen layer as determined from the 900 MHz reflection profiling. Good correlation between the GPR and impedance probe data can be seen with both images exhibiting very similar extent and shape the unfrozen zone, as well as corresponding gaps in the ground freezing. Further, good correlation can be seen in the March planviews given Figure 3.34. Once again, similar shapes and lateral extents of the unfrozen zone as well as continuity of the frost table were obtained from the two data sets.

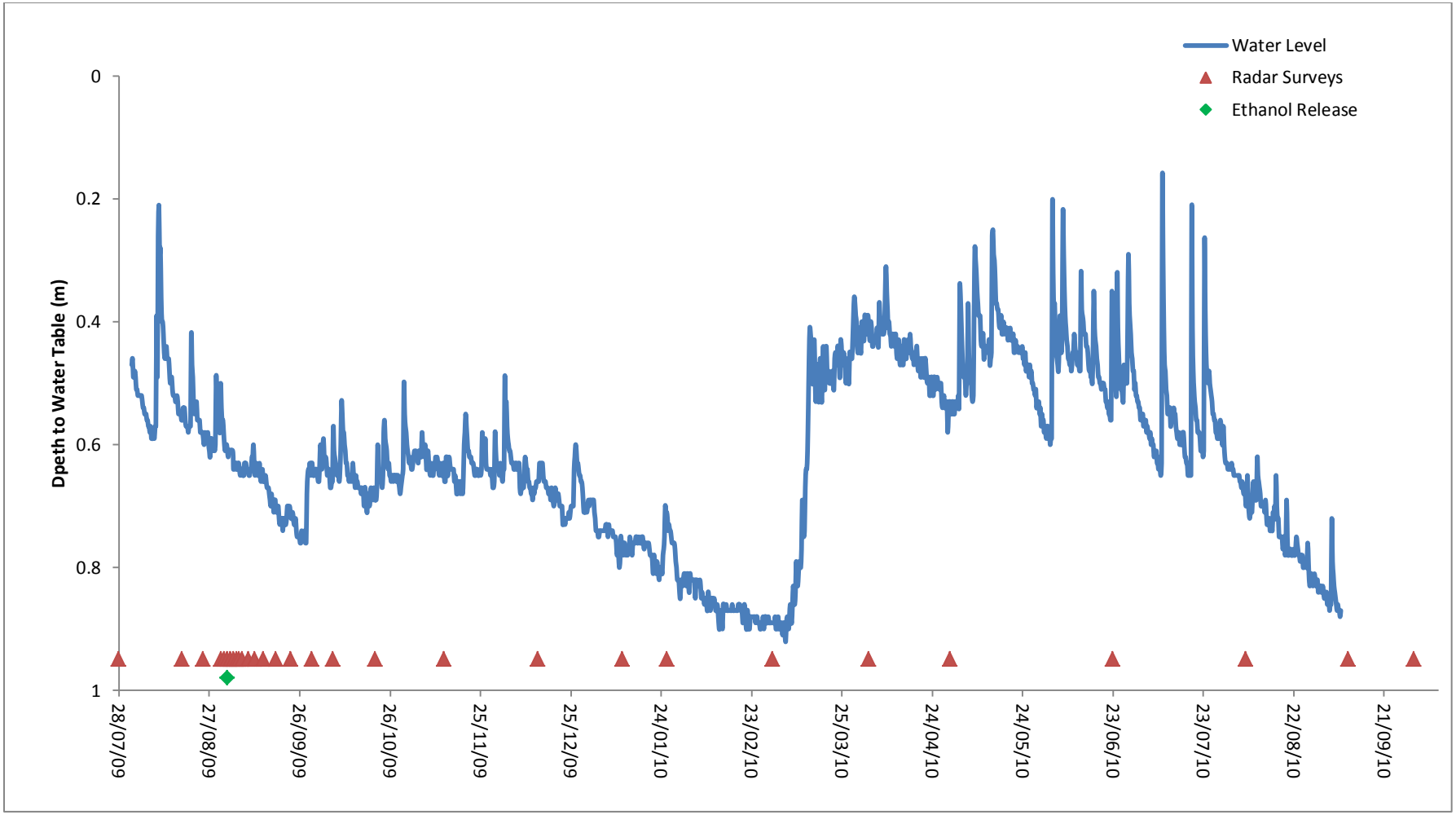

Figure 3.1 - Water table depths below the surface measured within the test cell over the course of the experiment (July 28, 2009 – October 1, 2010) with superimposed GPR survey dates.

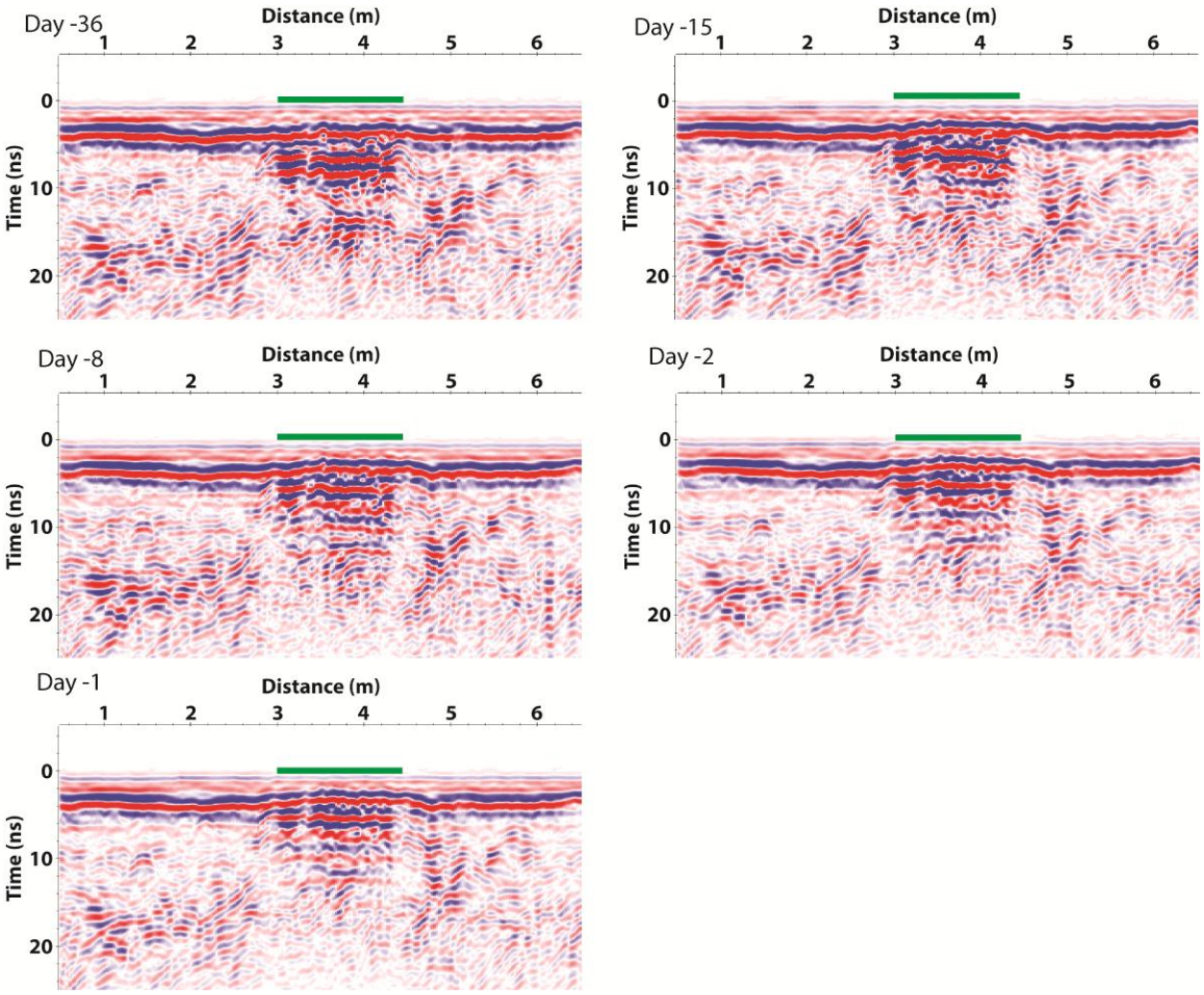

Figure 3.2 – Background 900 MHz radar profiles acquired between July 28 – September 1, 2009 along Line 3 showing emplaced gasoline residuals prior to ethanol release. The release trench is indicated by the green line.

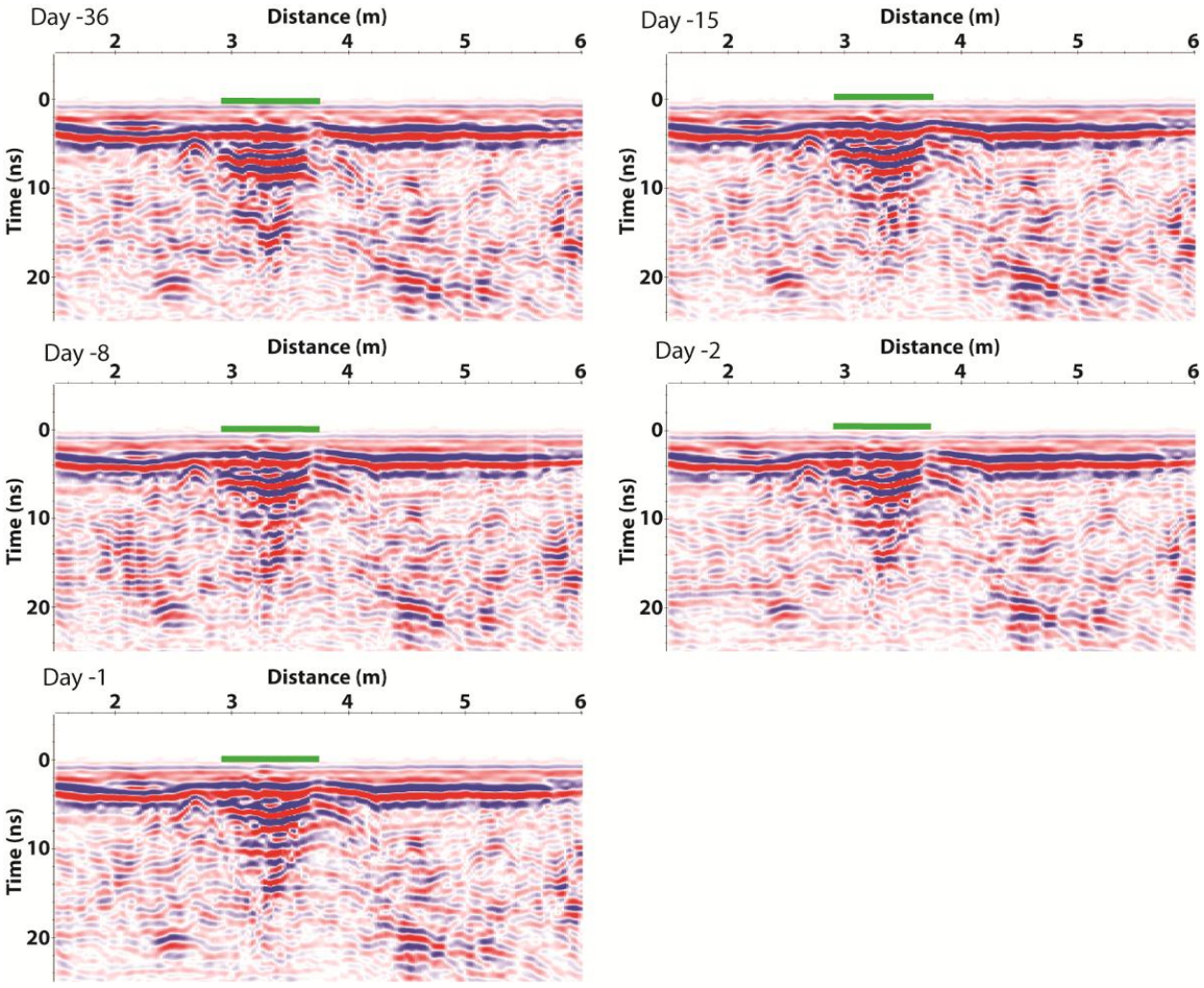

Figure 3.3 – Background 900 MHz radar profiles along Line B acquired between July 28 – September 1, 2009 showing emplaced gasoline residuals prior to ethanol release. The release trench is indicated by the green line.

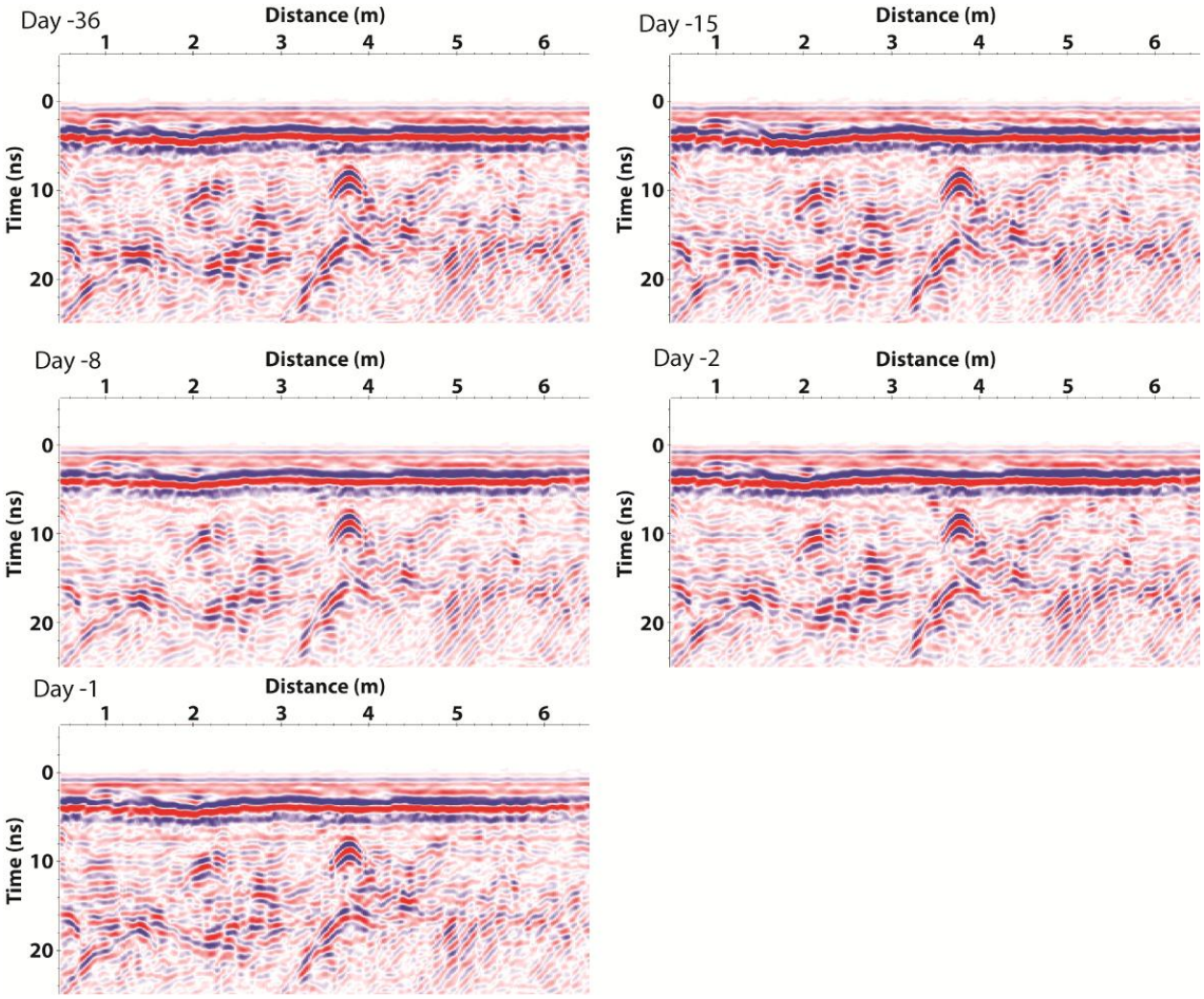

Figure 3.4 – Background 900 MHz radar profiles along Line 4 acquired between July 28 – September 1, 2009 showing the absence of indications of emplaced gasoline.

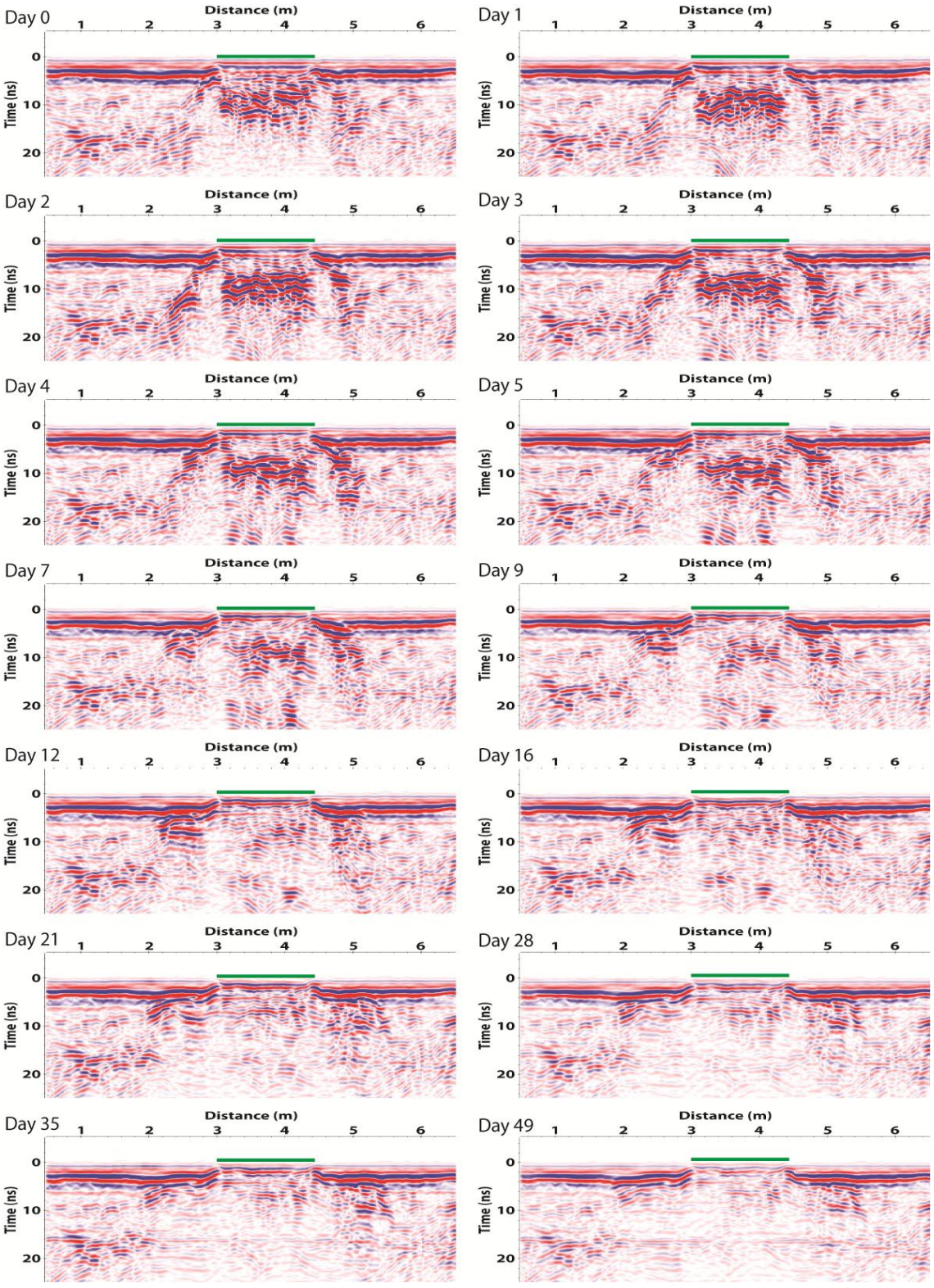

Figure 3.5 – 900 MHz radar profiles along Line 3 acquired between September 2 – October 21, 2009 showing the initial remobilization of the gasoline and expansion of the contaminated zone after the ethanol release. The release trench is indicated by the green line.

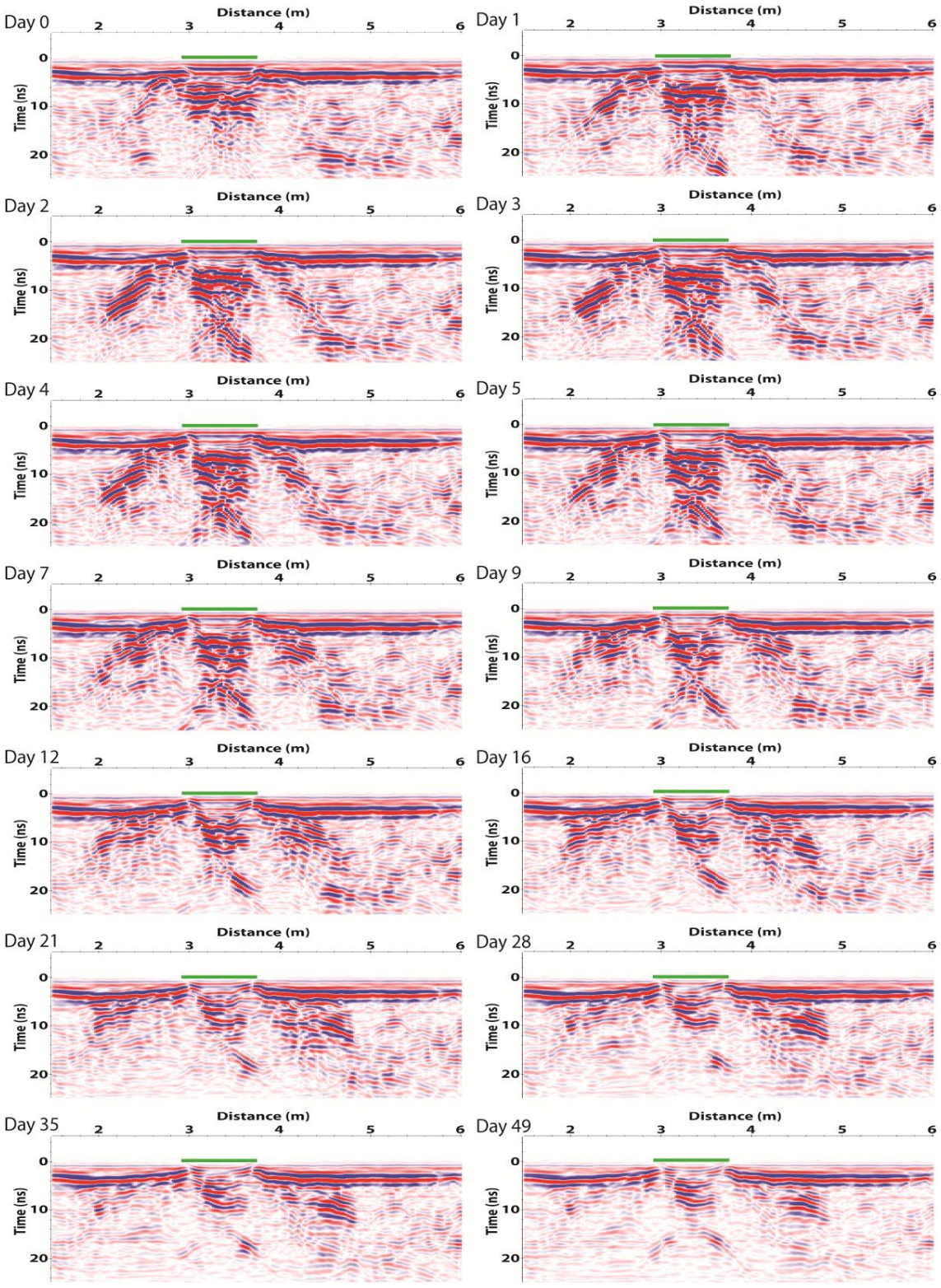

Figure 3.6 – 900 MHz radar profiles along Line B acquired between September 2 – October 21, 2009 showing the initial remobilization of the gasoline and expansion of the contaminated zone after the ethanol release. The release trench is indicated by the green line.

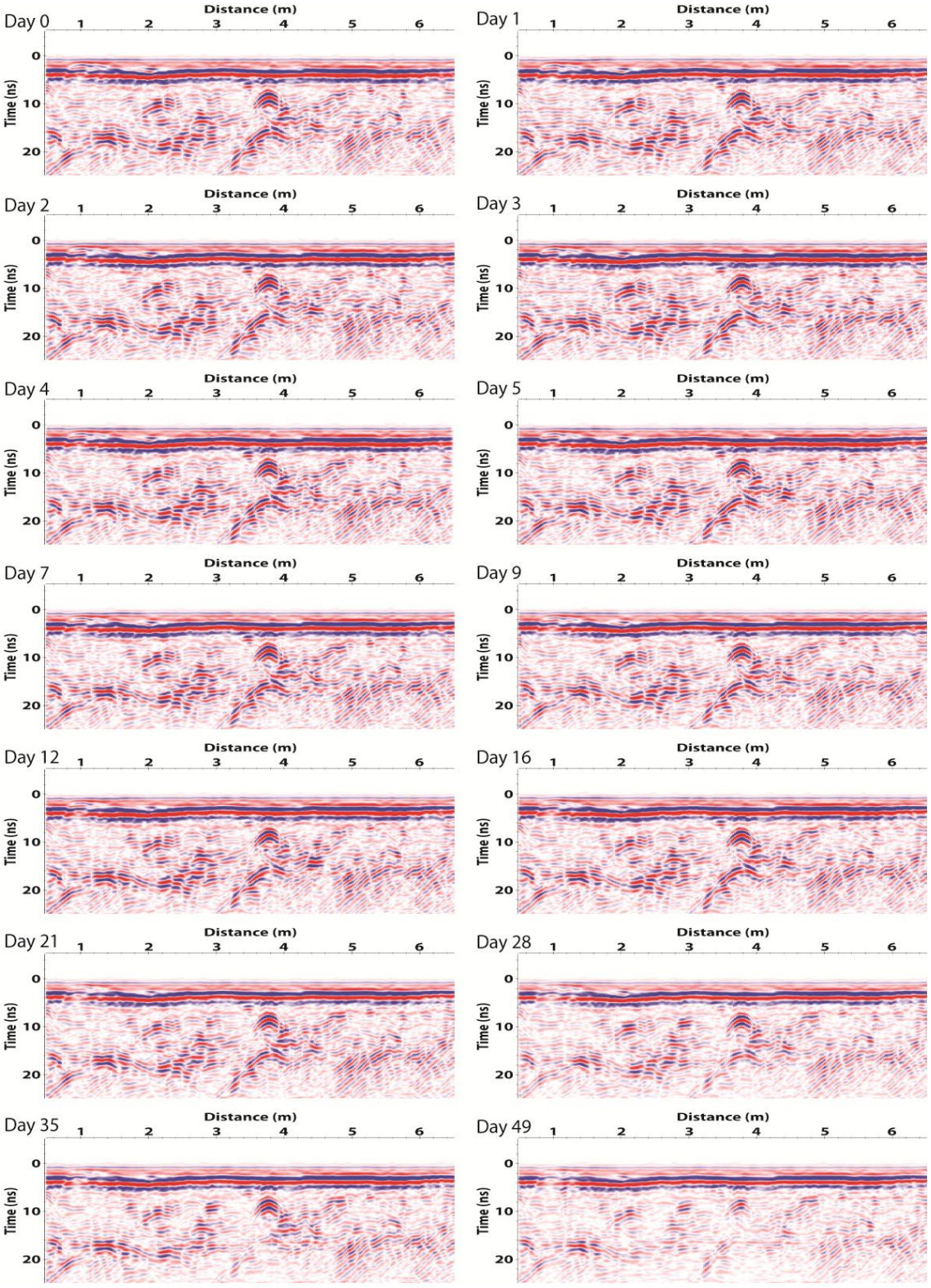

Figure 3.7 – 900 MHz radar profiles along Line 4, acquired between September 2 – October 21, 2009 showing the continued absence of contaminants after the ethanol release.

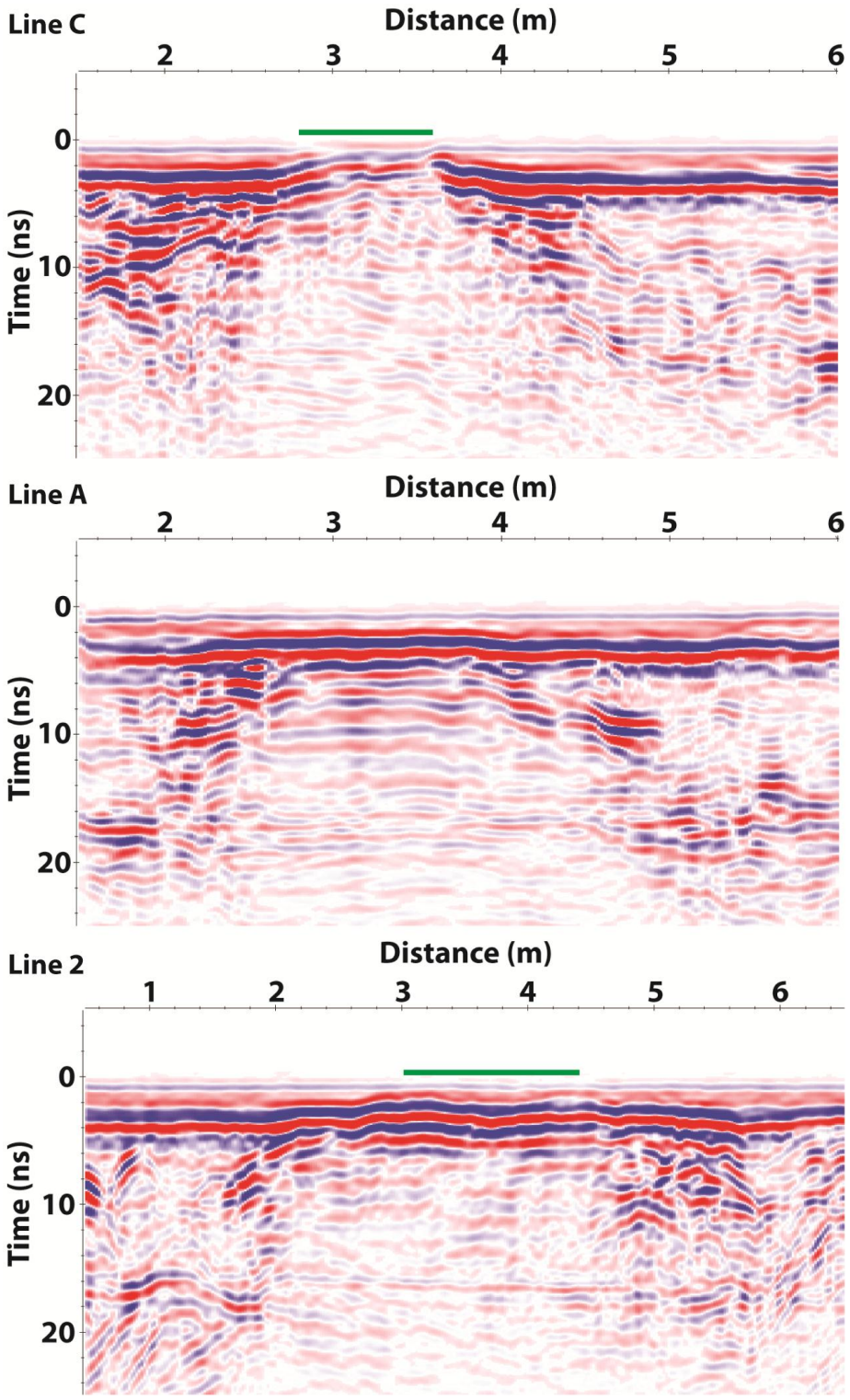

Figure 3.8 – 900 MHz profiles along Lines C, A, and 2, acquired on September 30, 2009. Showing the expansion of the gasoline/ethanol as high reflectivity near-surface events along the profiles.

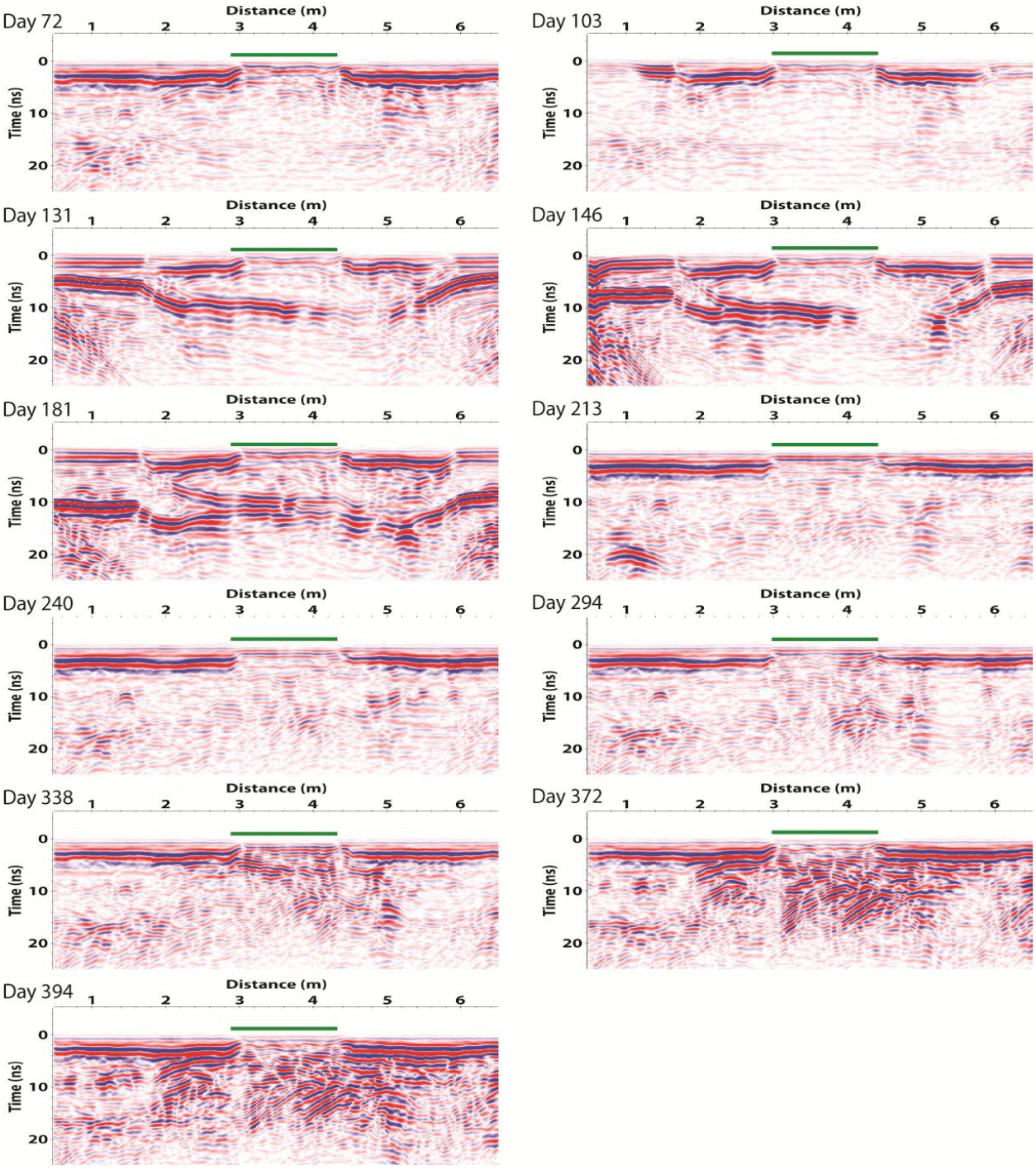

Figure 3.9 – 900 MHz radar profiles along Line 3 acquired between November 13, 2009 – October 1, 2010 showing the longer term evolution of the contaminant contaminated zone during changing seasonal conditions. The release trench is indicated by the green line.

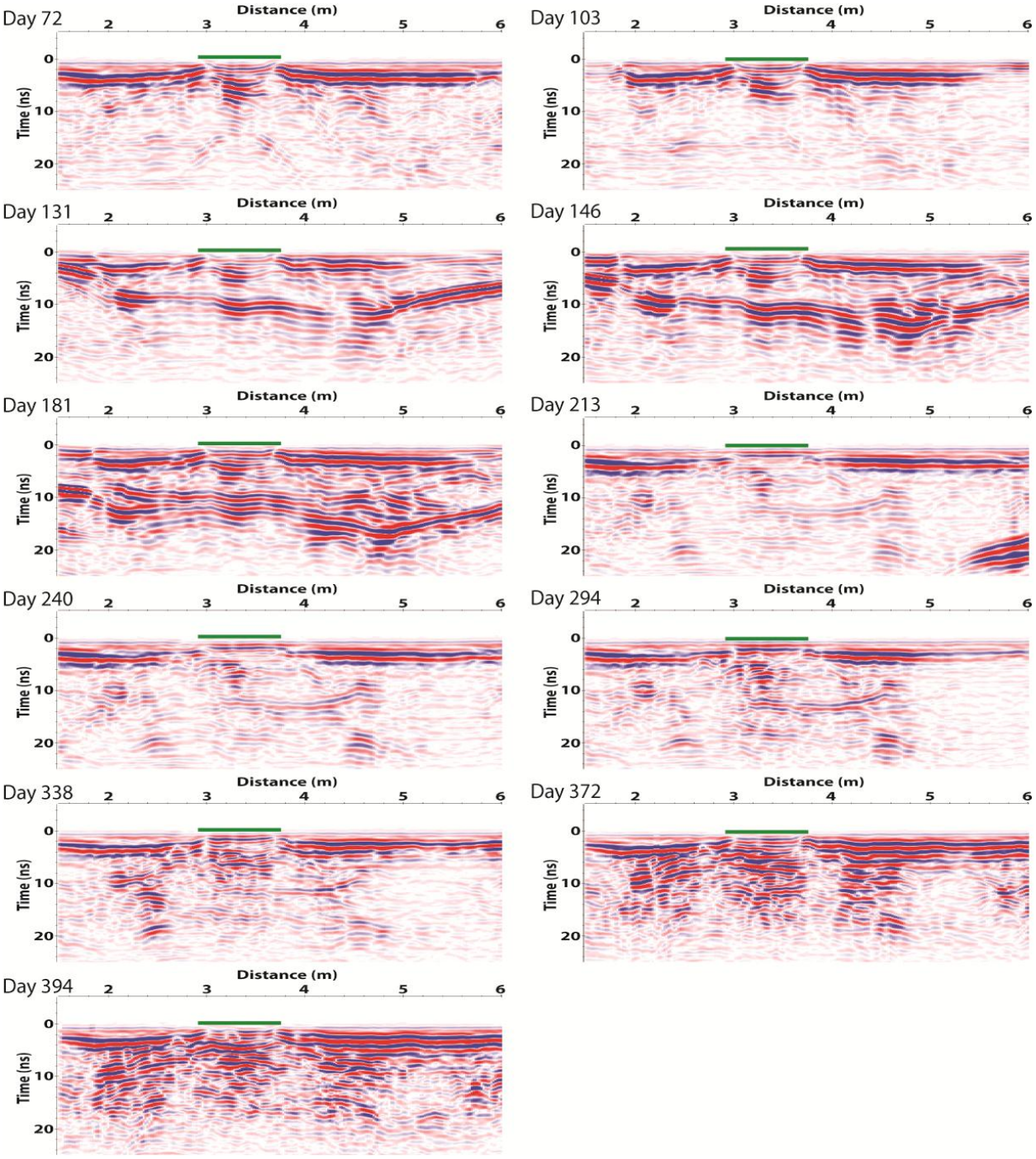

Figure 3.10 – 900 MHz radar profiles along Line B acquired between November 13, 2009 – October 1, 2010 showing the longer term evolution of the contaminant contaminated zone during changing seasonal conditions. The release trench is indicated by the green line.

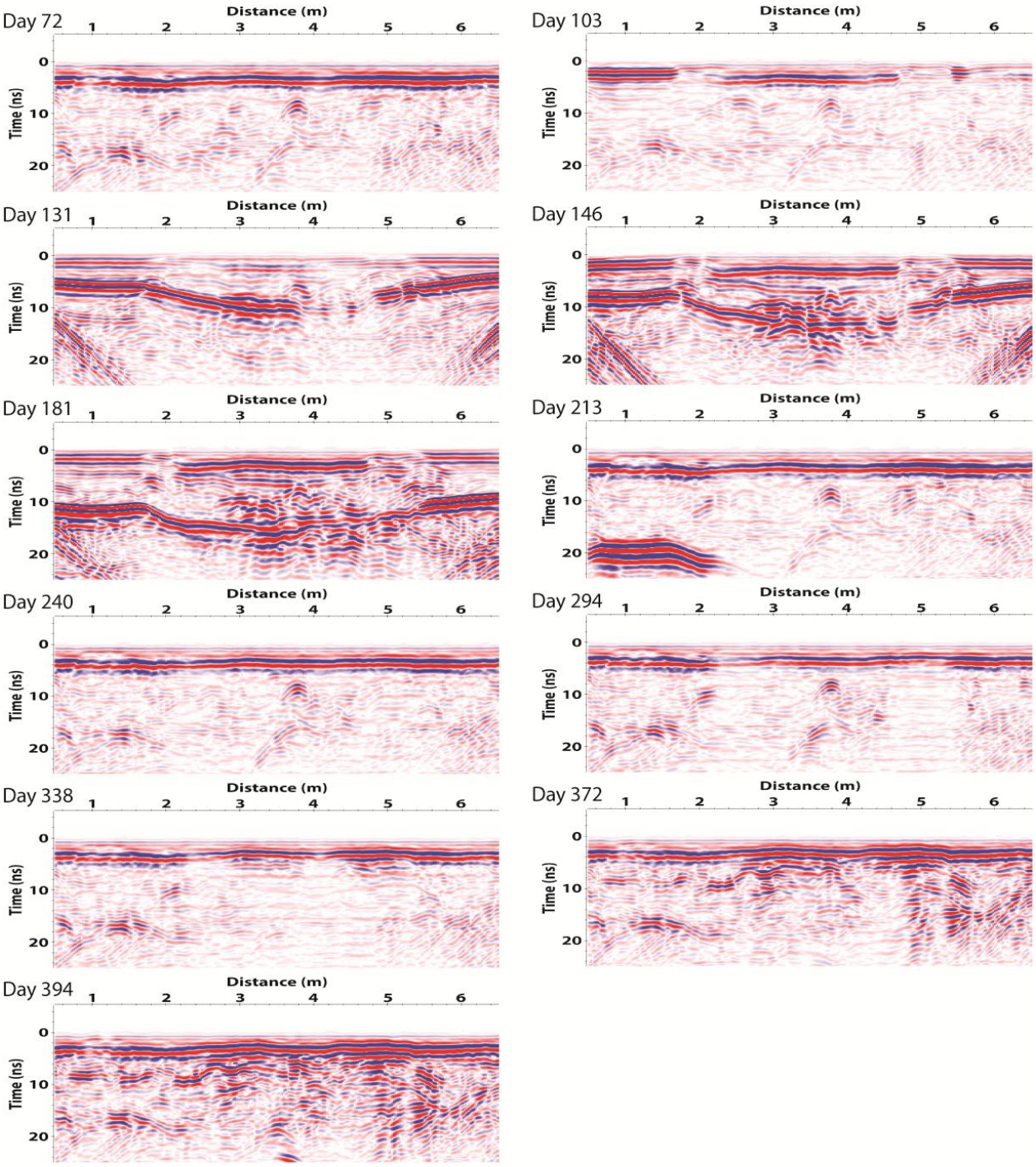

Figure 3.11 – 900 MHz radar profiles along Line 4 acquired between November 13, 2009 – October 1, 2010 showing the longer term development of the contaminant contaminated zone during changing seasonal conditions.

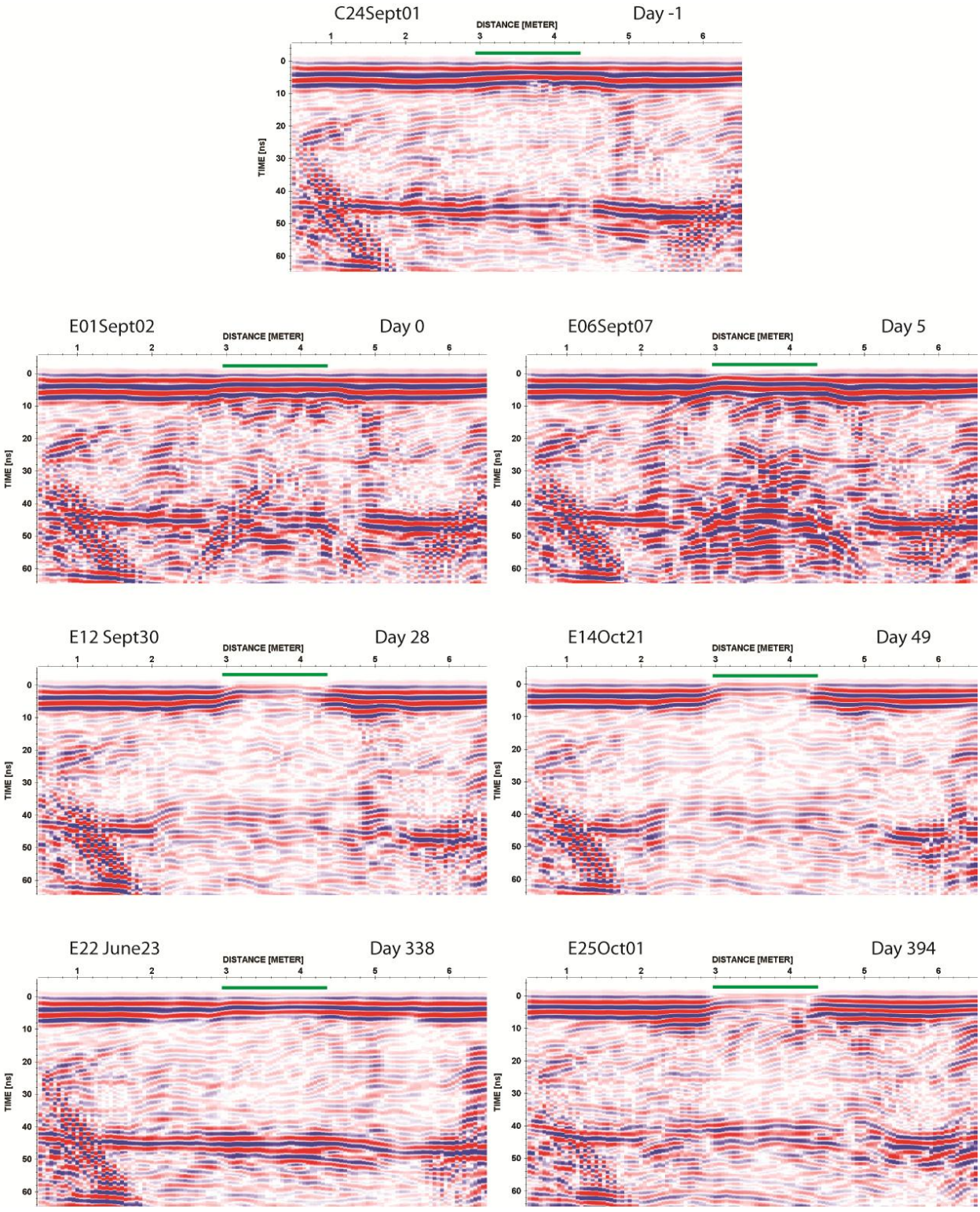

Figure 3.12 – 450 MHz radar profiles along Line 3 acquired during unfrozen conditions during the entire monitoring period showing the variation in traveltime for the underlying stratigraphic reflection at ~ 45 ns. The release trench is indicated by the green line.

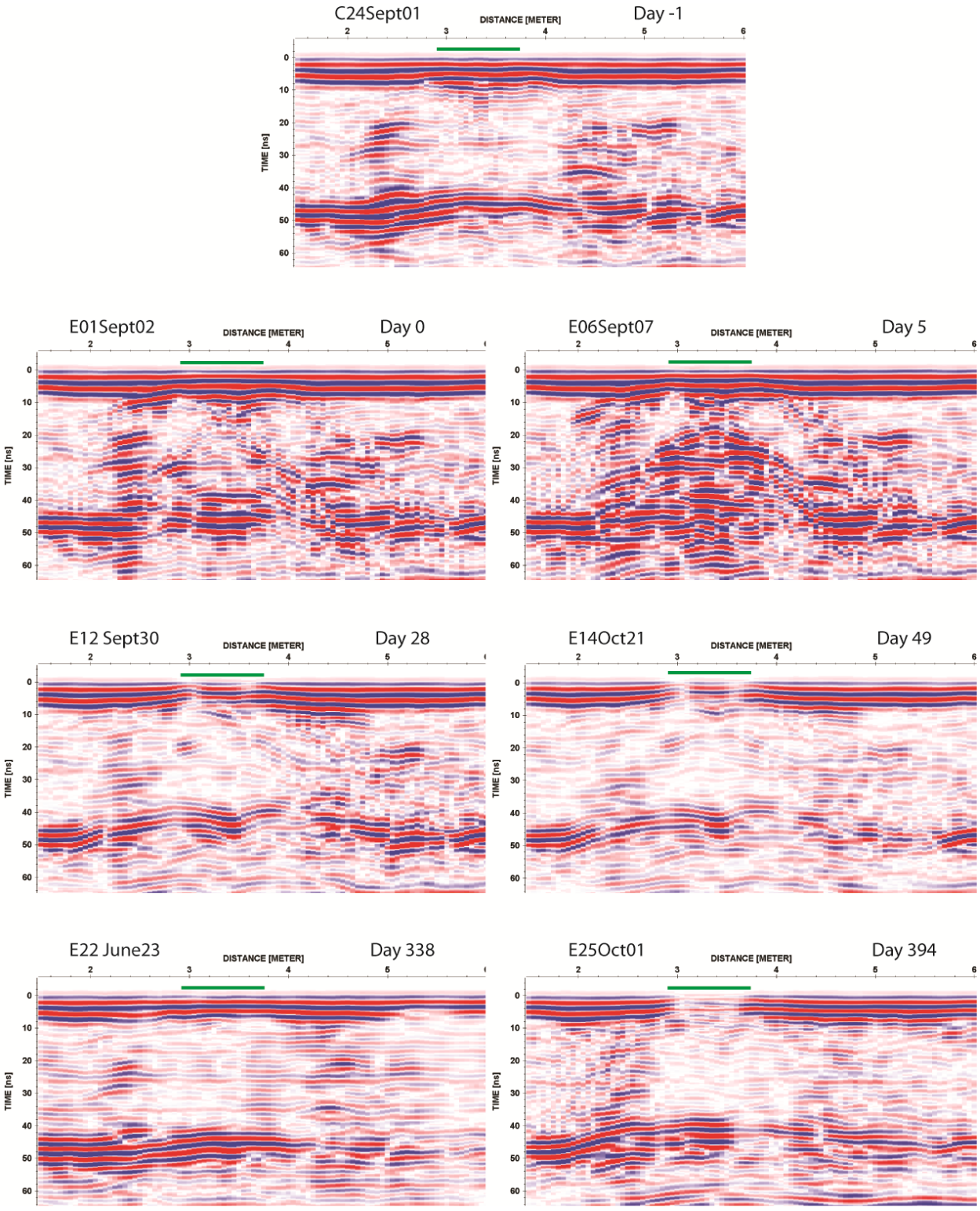

Figure 3.13 – 450 MHz radar profiles along Line B acquired during unfrozen conditions during the entire monitoring period showing the variation in traveltime for the underlying stratigraphic reflection at ~ 45 ns. The release trench is indicated by the green line.

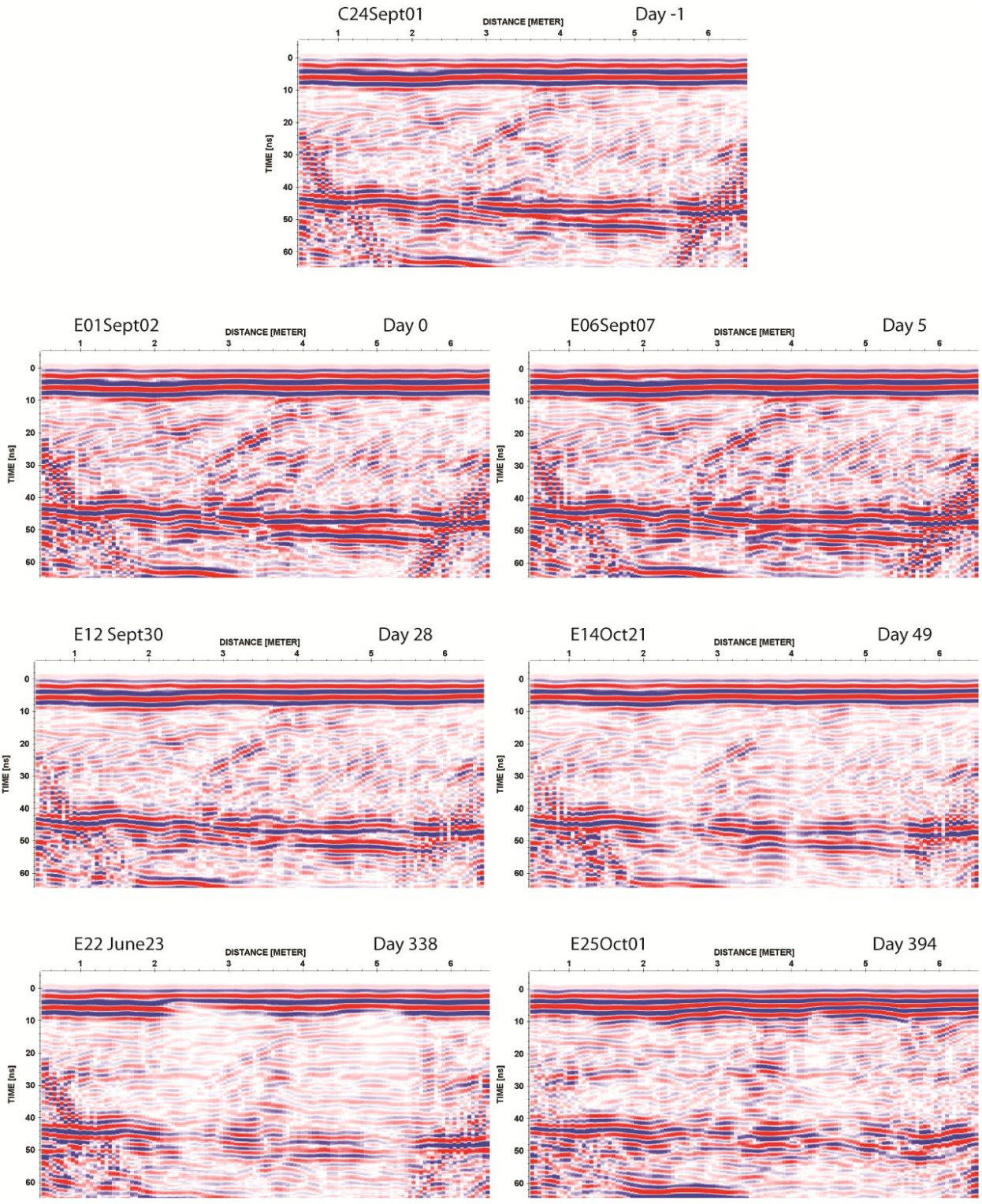

Figure 3.14 – 450 MHz radar profiles along Line 4 acquired during unfrozen conditions during the entire monitoring period showing the variation in traveltime for the underlying stratigraphic reflection at ~ 45 ns.

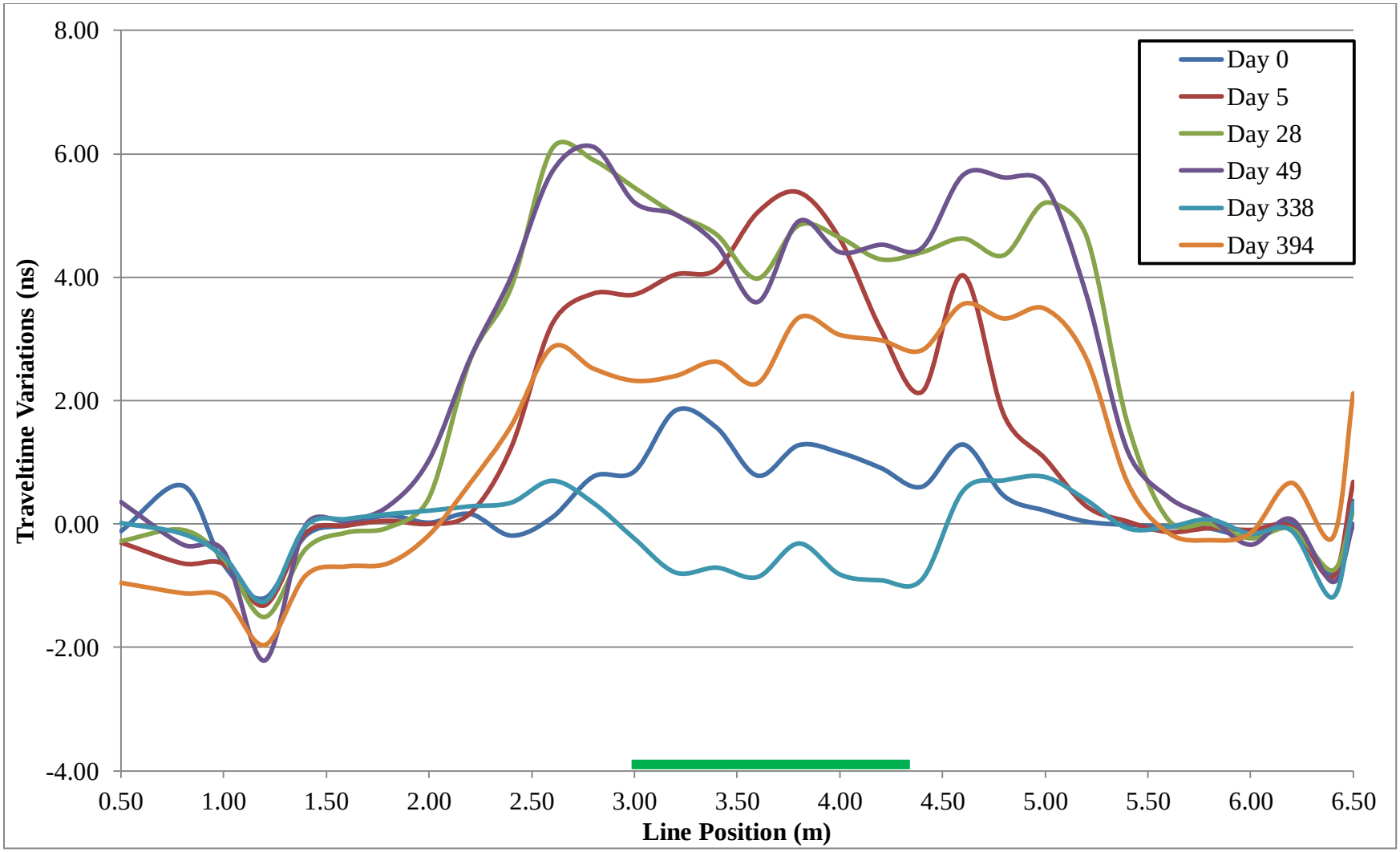

Figure 3.15 – Traveltime differences relative to Day -1 for the underlying stratigraphic reflection along Line 3 with the 450 MHz GPR antennae. The location of release trench is indicated by the green line.

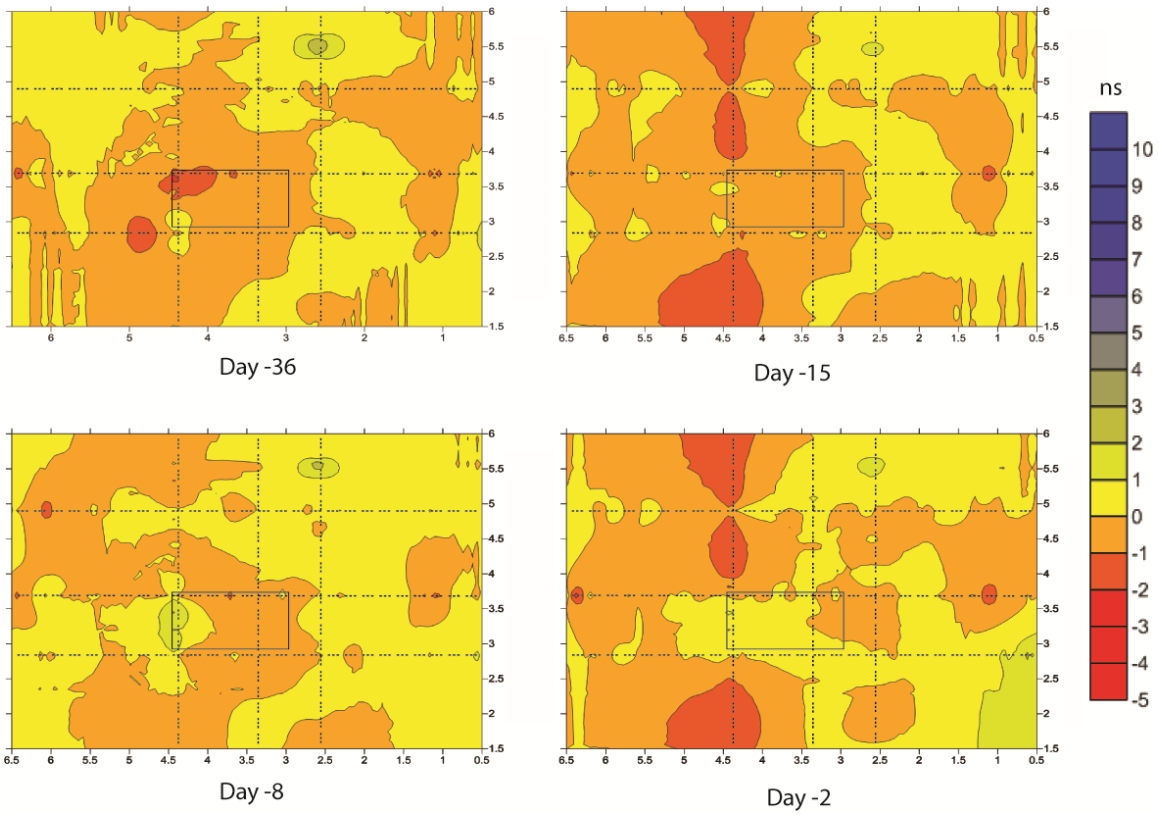

Figure 3.16 – Plan view of the traveltime difference relative to Day -1 (September 1, 2009) for the underlying stratigraphic reflection during the pre-release period (July 28-August 31, 2009). Locations of GPR profiles lines (dashed) and release trench (solid) are shown.

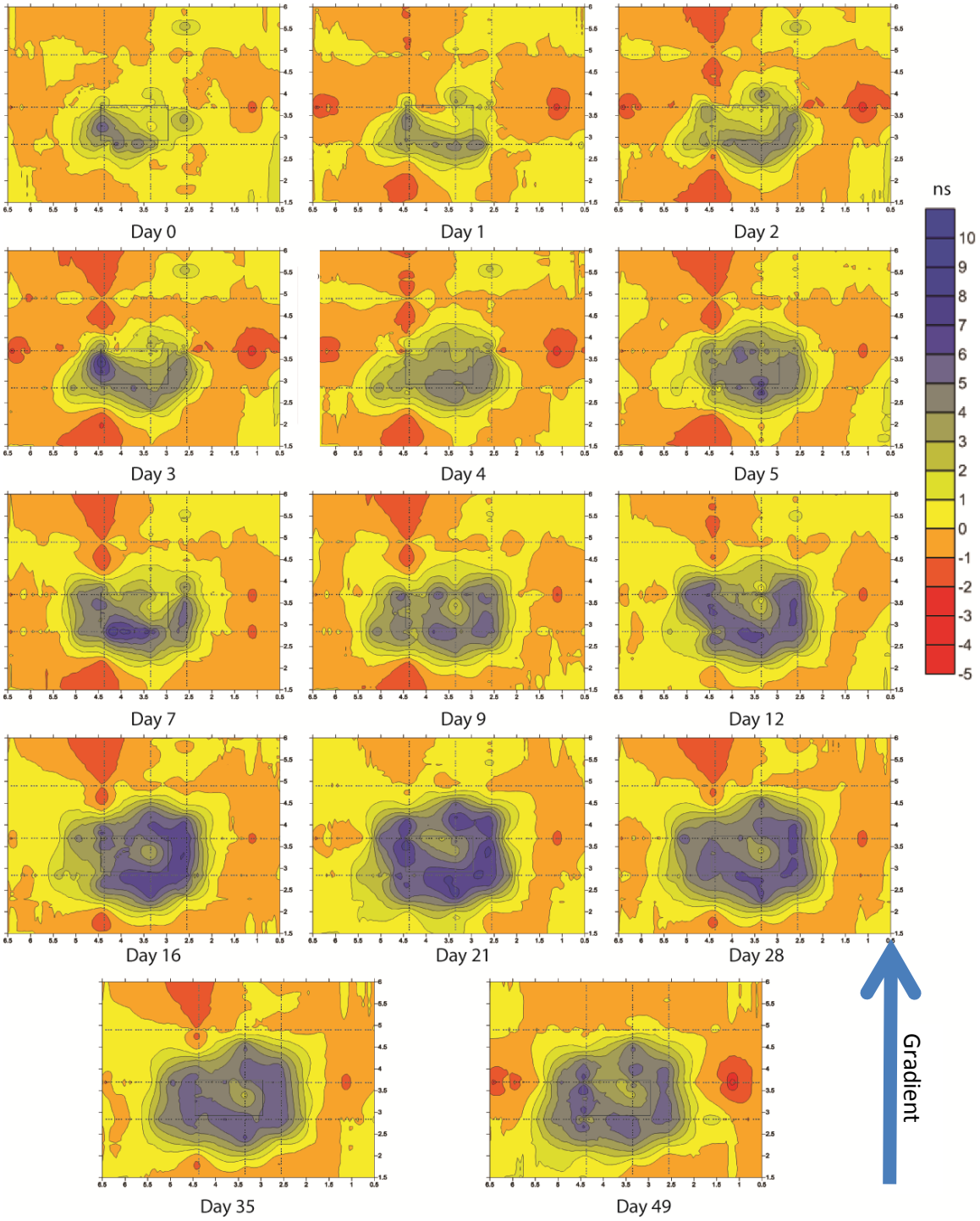

Figure 3.17 – Plan view of the traveltime difference relative to Day -1 (September 1, 2009) for the underlying stratigraphic reflection during the initial post-release period (September 2-October 21, 2009). Locations of GPR profiles lines (dashed) and release trench (solid) are shown. Direction of ground water flow as indicated.

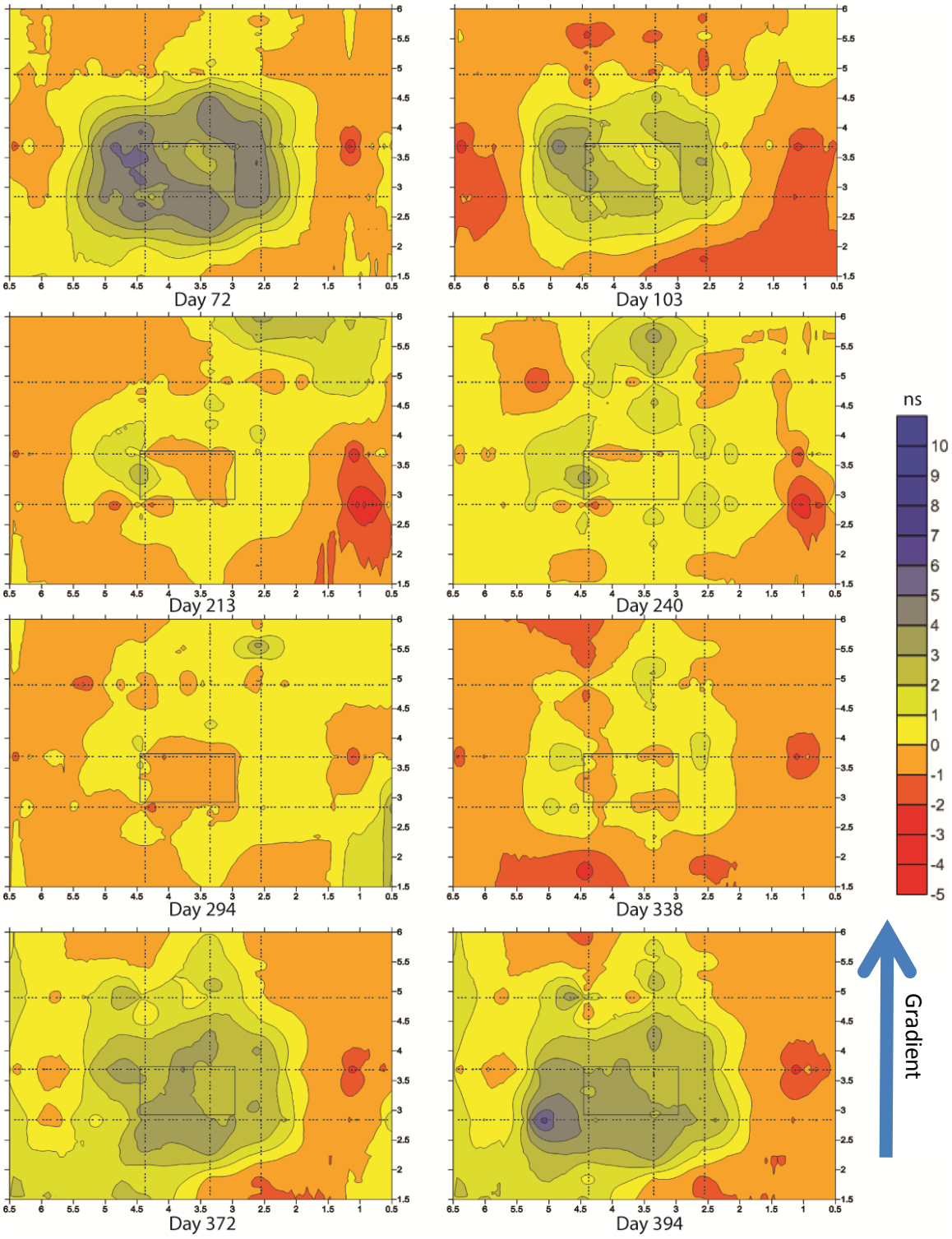

Figure 3.18 – Plan view of the traveltime difference relative to Day -1 (September 1, 2009) for the underlying stratigraphic reflection during the longer term post-release period (November 13, 2009-October 1, 2010). Locations of GPR profiles lines (dashed) and release trench (solid) are shown. Direction of ground water flow as indicated.

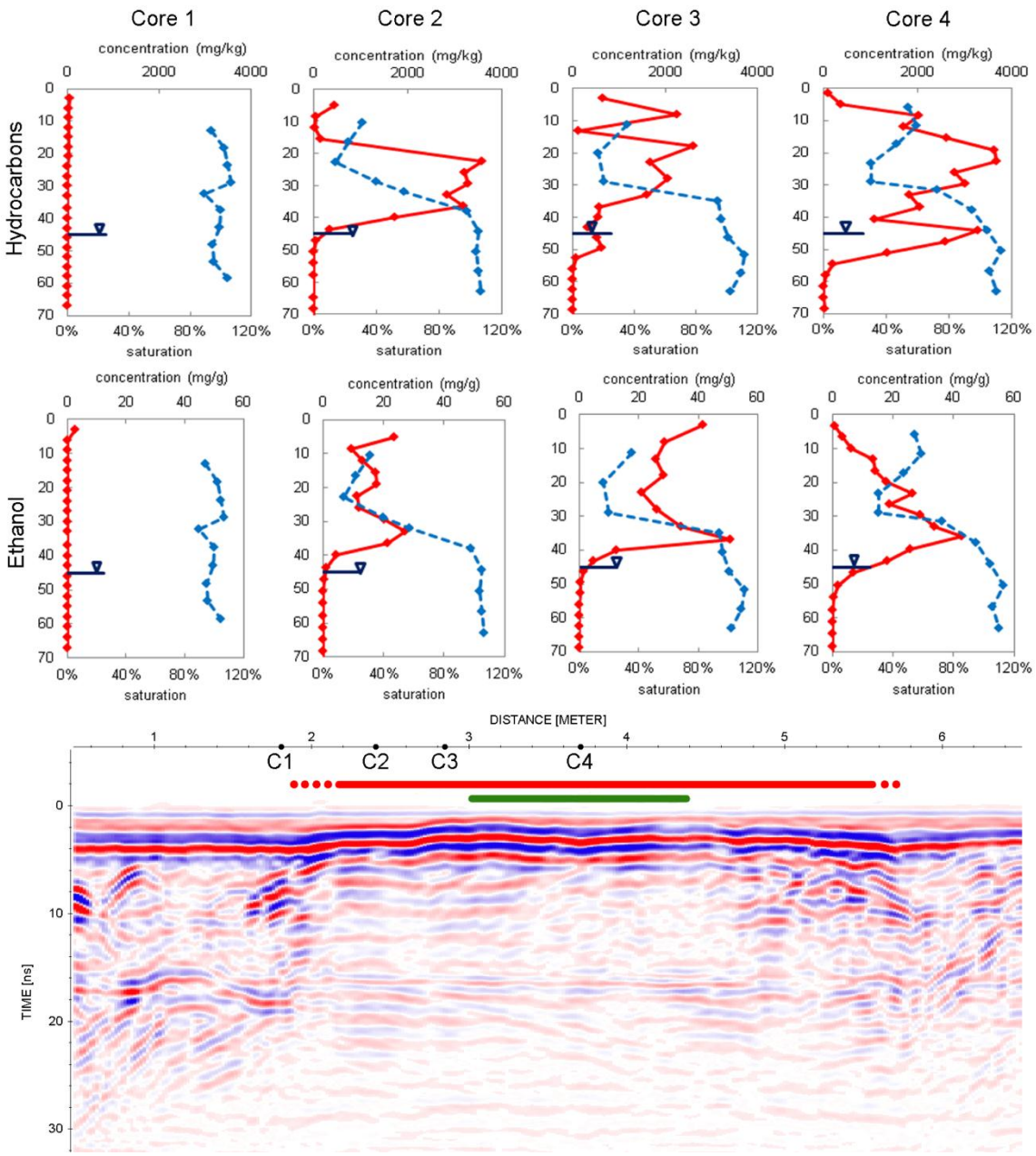

Figure 3.19 - Comparison between 900 MHz reflection profiling along Line 2 and results from soil cores (contaminant concentration shown in red and water saturations shown in blue). Extent of near-surface reflection event is shown in red (horizontal portion-solid, dipping-dots). Core locations are indicated on profile.

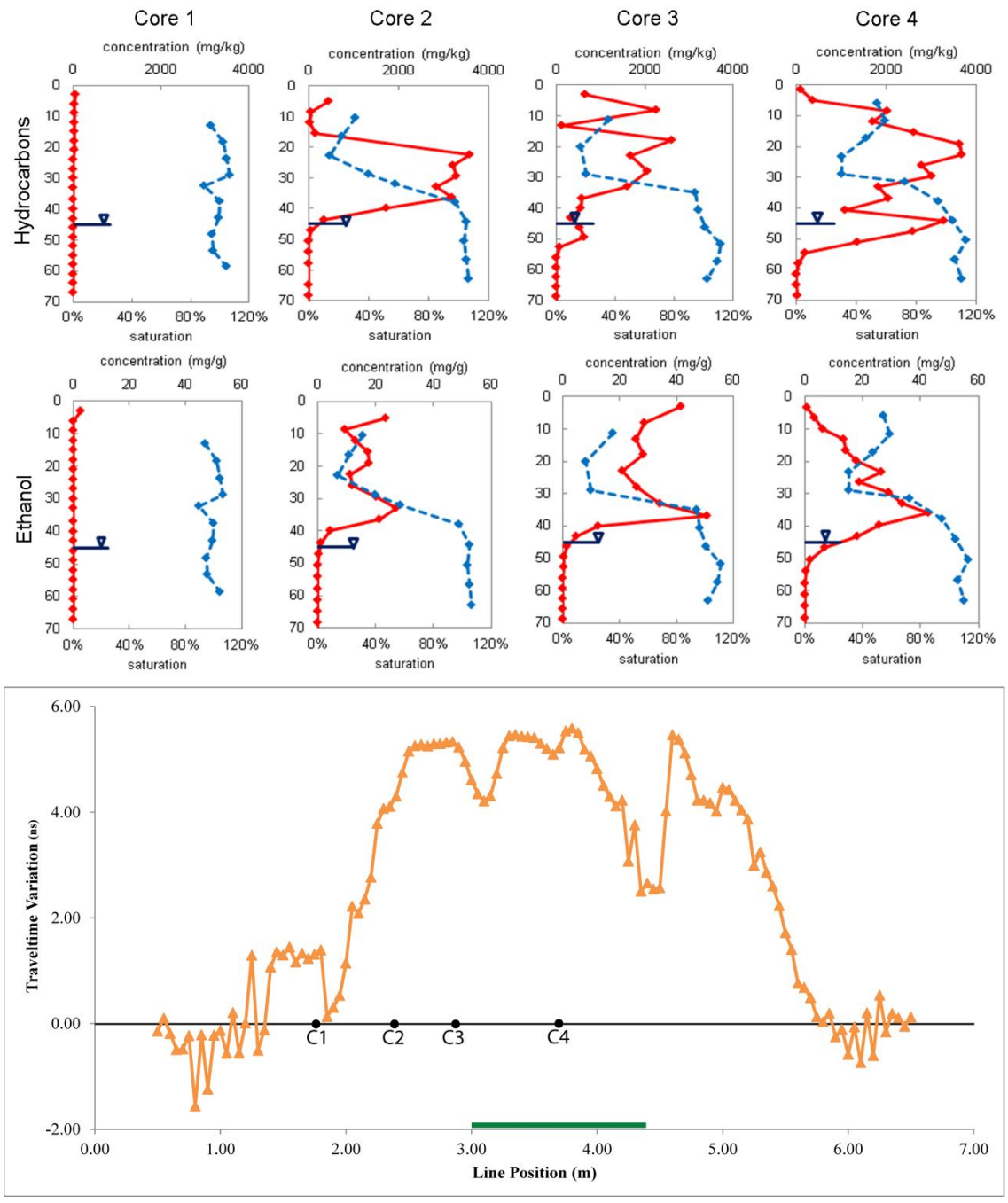

Figure 3.20 - Comparison between 450 MHz traveltime differences for underlying stratigraphic reflection along Line 2 and results from soil cores (contaminant concentration shown in red and water saturations shown in blue). Core locations are indicated on profile. The extent of release trench is shown in green.

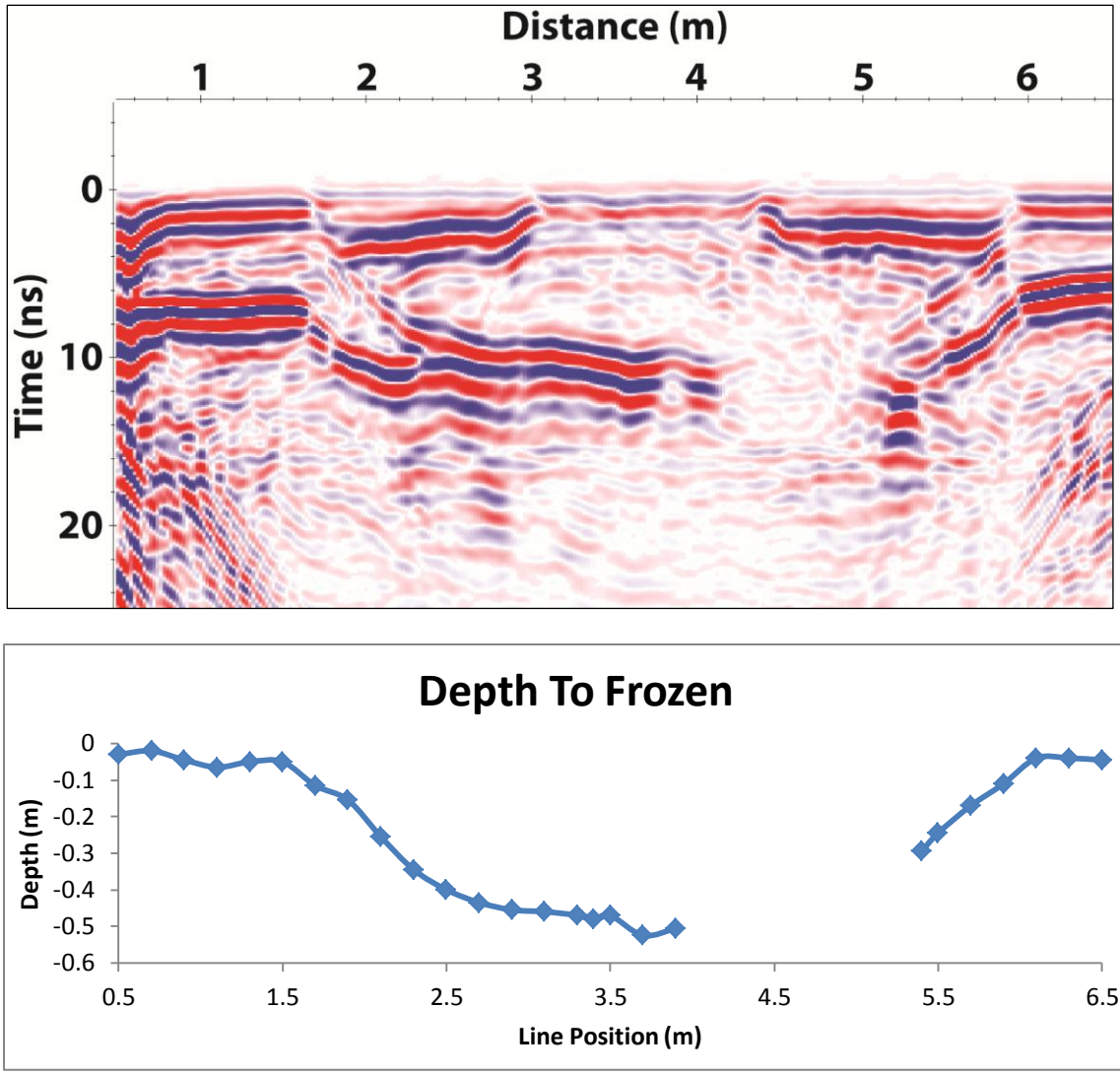

Figure 3.21 – Correlation of the 900 MHz depressed frozen layer and the depths determined from the ground probing rod along Line 3. Both data sets collected January 26, 2010.

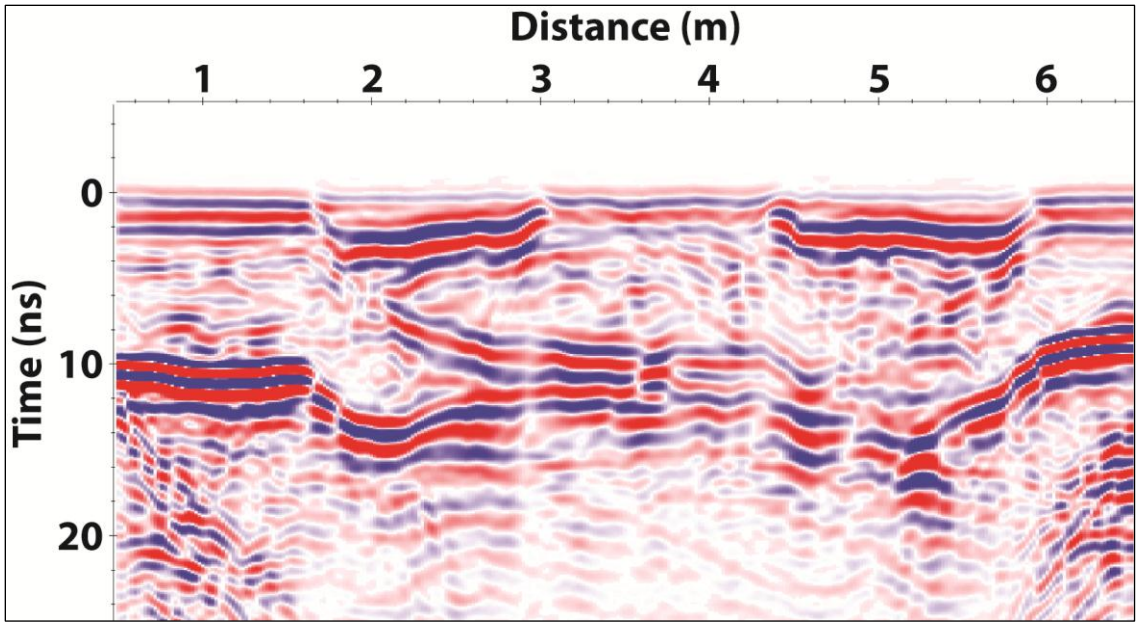

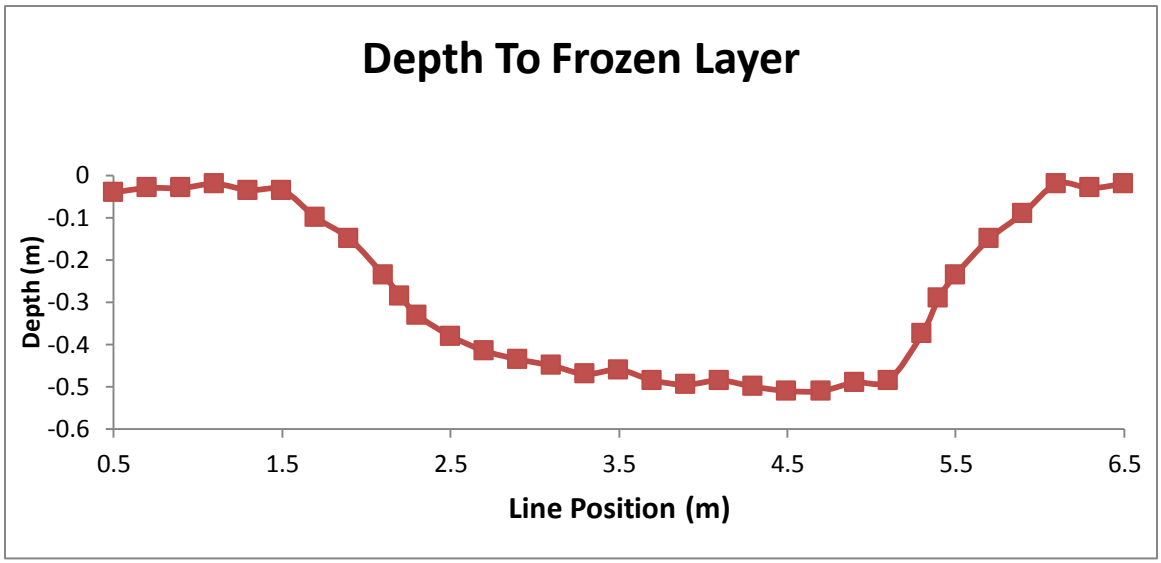

Figure 3.22 – Correlation of the 900MHz depressed frozen layer and the depths determined from the ground probing rod along Line 3. The GPR reflection profile was collected March 02, 2010, and the depth to frozen layer data collected March 08, 2010.

GPR traveltime to frozen layer

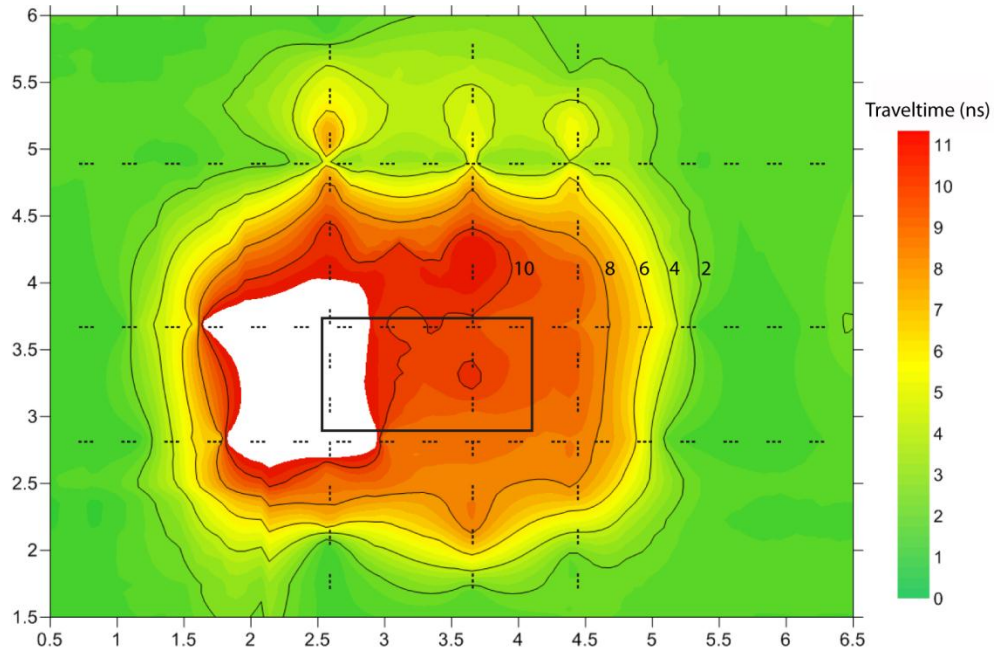

Impedance depth to frozen layer

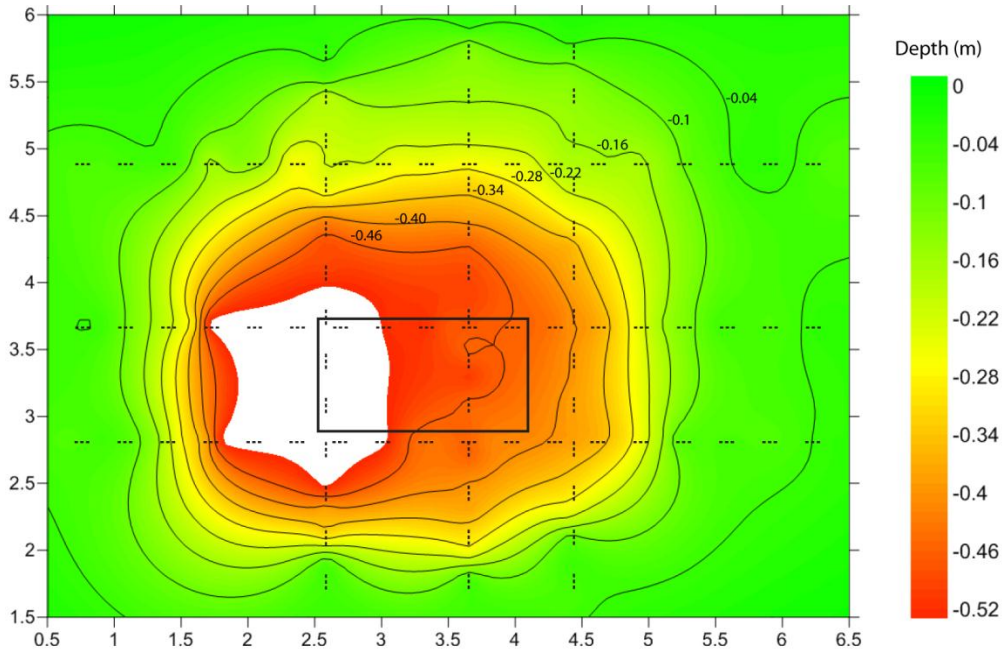

Figure 3.23 – Interpolated depth to the frozen layer as observed through the ground probing rod and the 900 MHz traveltime data. White indicates area where soil freezing was not detected by probe or reflection was not present in GPR profiling. Data was collected January 26 2010.

GPR traveltime to frozen layer

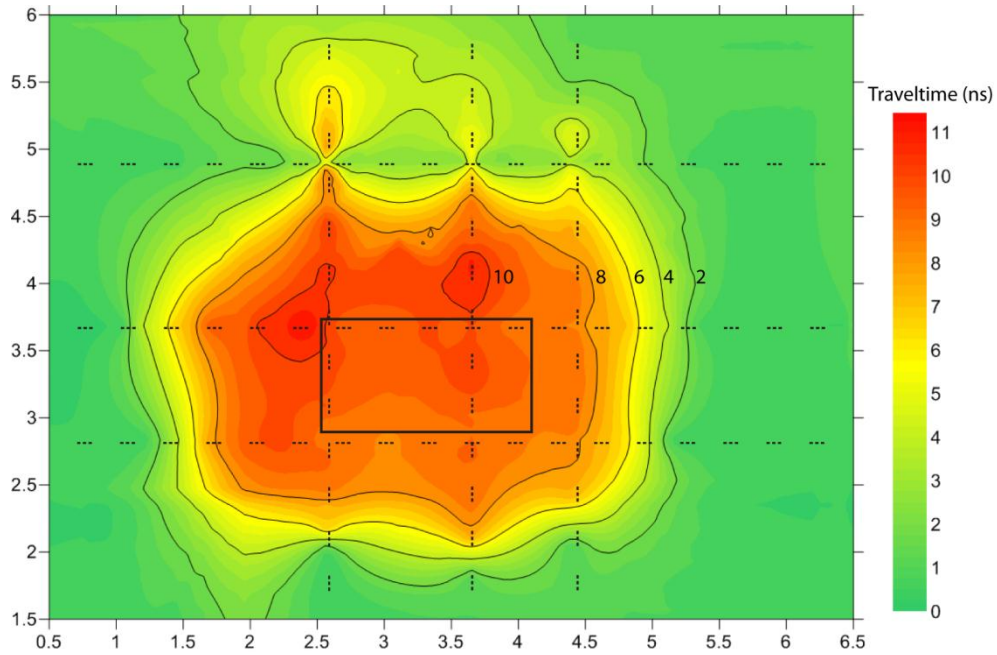

Impedance Depth to frozen layer

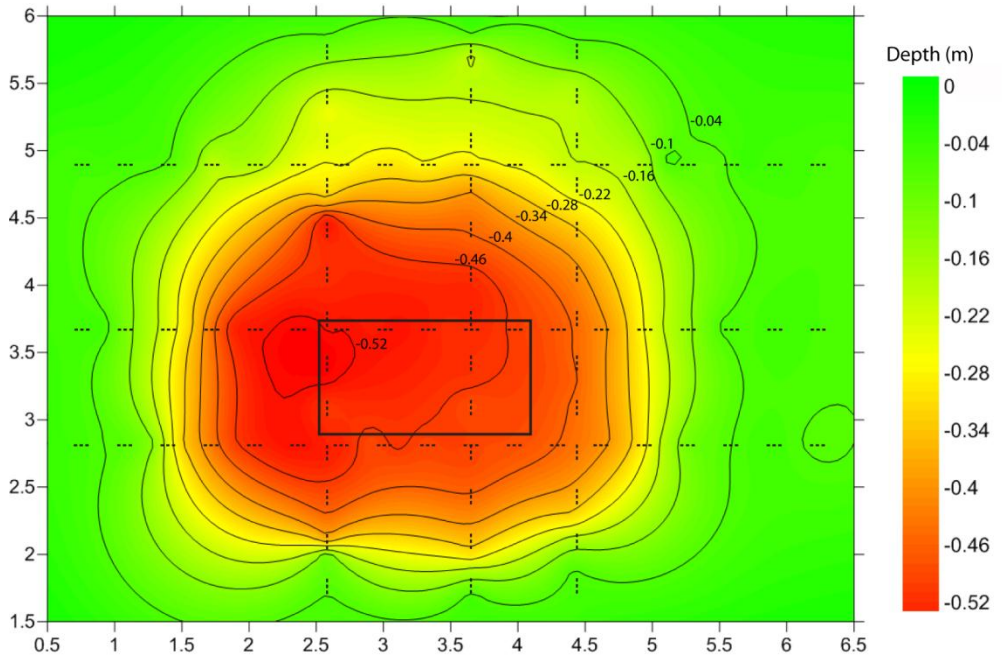

Figure 3.24 – Interpolated depth to the frozen layer as observed through the ground probing rod showing good correlation to the 900 MHz traveltime to the frozen layer. GPR and impedance data collected March 02 and March 08, 2010 respectively.

4.0 Conclusions

The objective of this study is to add to our current knowledge and guide future research into gasoline/ethanol interactions. To that end, the results show significant potential for GPR in monitoring the redistribution of gasoline residuals as a result of a subsequent ethanol release. This research is unique in that the controlled release of ethanol into gasoline residuals has not been previously monitored using geophysical techniques at either the laboratory or field scale. Despite this being a relatively small release compared to potential actual releases, the GPR reflection profiling was able to detect and monitor significant changes in the reflectivity of the shallow contaminated zone. From changes in shallow reflectivity amplitudes and reflection event travel times from an underlying stratigraphic interface, the location and extent of the contaminant pool was easily delineated and its evolution monitored over time.

Due to the very shallow depth of the gasoline/ethanol contaminated zone, the higher resolution of the 900 MHz reflection data was required to minimize the interference due to the superposition of the direct ground wave. The early time 900 MHz reflection profiling (Days 0-50) clearly observed the remobilization of the gasoline after the ethanol release. For the first 7 days immediately after the release, the pre-existing high-amplitude events below the release trench associated with the initial gasoline release appeared to shift downwards and marginally contract laterally; this response is consistent with laboratory observations of ethanol-induced redistribution of gasoline. Afterward, these events below the release trench dissipated, suggesting a co-solvency effect due to the presence of the ethanol or remobilization of the existing gasoline.

During this time, the 900 MHz reflection profiling also shows the formation of high-amplitude, shallow reflection events along the trench periphery that progressively move laterally outwards from the trench area as the water table dropped. The lateral expansion of the events reached their observed maximum extent on Day 28, corresponding with the water table's lowest point. This lateral extent was greater than that observed during the original gasoline release the previous year. The correlation between these reflection events and the presence of the gasoline/ethanol contaminated zone was supported by soil cores acquired during this period.

The onset of winter conditions induced significant changes which were imaged in the subsurface by the 900 MHz reflection profiling. This profiling indicated that the seasonal freezing process was significantly influenced by the presence of the gasoline/ethanol contaminated zone. In addition, variations in the direct ground wave event suggest that this contaminated zone extended up to the surface. Two series of direct impedance probing with a steel rod found that the material in region of anomalous GPR response was unfrozen. It is reasonable to assume that the presence of the ethanol and gasoline inhibited the development of frozen soil due to their significantly lower freezing points.

The geometry of the unfrozen zone as defined by the probing was well-imaged by the reflection profiling. This unfrozen zone had significantly larger areal extent than the contaminated zone inferred from the 900 MHz profiling done before winter. In particular, reflection profiling and ground probing showed that the unfrozen zone extended down gradient to Line 4, where there was no previous indication of contaminant impact. A possible cause for the larger extent of the unfrozen zone is that the content of dissolved ethanol in the groundwater was sufficient to inhibit pore water freezing but did not greatly change the dielectric permittivity

of the system. This condition is feasible given the relatively low contrast in permittivity between ethanol and water (i.e., $\kappa \sim 25$ versus $\kappa \sim 80$) compared to other components.

After the spring melt and the subsequent rise of the water table there was little, if any, evidence of the gasoline/ethanol contaminated zone on the 900 MHz reflection profiles. However, high-reflectivity events gradually redeveloped as the water table dropped. The lateral extent of these events corresponded with the location of the unfrozen soil and hence was greater than that of the immediate post-release events imaged on Day 28. As with the freezing anomalies, these events were also observed on the down-gradient Line 4, which appeared unaffected prior to winter. While the cause of these events is not well understood, it can be hypothesized that they might be the result of differential drainage due to the presence of ethanol. Further analysis should be performed on evaluating the effects of biodegradation as well as quantifying the amount and rate of hydrocarbon removal below the release trench following the release.

Due to its lower resolution and the resulting superposition of the direct ground wave, the 450 MHz reflection profiling did not image the shallow contaminated zone as well as the 900 MHz profiles. However, the greater depth of penetration achieved with the lower frequency 450 MHz system permitted the imaging of an underlying stratigraphic boundary that was used to infer the presence of contaminants through velocity effects on the reflection event traveltimes (i.e., "velocity pull-up"). By using the 450 MHz profiling immediately before the ethanol release as the reference data set, these traveltime differences should indicate effects of the release on subsurface conditions. These traveltime results indicate an evolution of the contaminated zone that is consistent with 900 MHz results during periods of unfrozen conditions: (1.) the initial development and lateral spreading of the contaminated zone after the release and during the

falling water table; (2.) the gradual reduction before winter and (3.) the progressive reappearance with increased spatial extent during the seasonal water table decline during the following summer.

The results presented in this thesis clearly demonstrate the capacity of high-frequency ground penetrating radar to detect and monitor very shallow zone (i.e., less than 1.0 meter depth) that have been contaminated by gasoline and ethanol releases. However, it is also apparent that further work is required to enable the extraction of quantitative information concerning the distribution and saturation of these contaminants in this natural system. It is hoped that this experiment provides the data and impetus for this work.

References

Abdul A.S., Gillham R.W., 1989. Field studies of the effects of the capillary-fringe on streamflow generation. Journal of Hydrology, 112(1-2), 1-18.

Annan, A.P., 2005a. Chapter 11: Ground penetrating radar, *in* Butler D.K. (editor), Near-surface geophysics. Society of Exploration Geophysicists, Tulsa, OK., 357 – 438.

Annan, A.P., 2005b. Chapter 7: Ground penetrating radar methods in hydrogeological studies, *in* Rubin Y. and Hubbard S.S. (editors), Hydrogeophysics. Springer, Dordrecht, NL., 185 – 213.

Annan, A.P., 2009. Chapter 1: Electromagnetic principles of ground penetrating radar, *in* Jol H.M. (editor), Ground Penetrating Radar: Theory and Applications. Elsevier, Amsterdam, NL. 3 – 40.

Arcone, S. A., and A. J. Delaney, 2003, Radiowave pulse refraction and ground wave propagation through permafrost and the active layer: Proceedings of the Eighth International Conference on Permafrost, International Permafrost Association, 21–26.

Atekwana E.A., Sauck W.A., Werkema Jr D.D., 2000. Investigations of geoelectrical signatures at a hydrocarbon contaminated site. Journal of Applied Geophysics, 44, 167-180.

Atekwana E.A., Atekwana E.A., 2010. Geophysical signatures of microbial activity at hydrocarbon contaminated sites: A Review. Surveys in Geophysics, 31, 247-283.

Bano M., Loeffler O., Girand J., 2009. Ground penetrating radar imaging and time-domain modeling of the infiltration of diesel fuel in a sandbox experiment. C.R. Geoscience

Bell L.S., Devlin J.F., Gillham R.W., Binning P.J., 2003. A sequential zero valent iron and aerobic biodegradation treatment system for nitrobenzene. Journal of Contaminant Hydrology, 66(3-4), 201-217.

Bermejo J.L., Sauck W.A., Atekwana E.A., 1997. Geophysical discovery of a new LNAPL plume at the former Wurtsmith AFB, Oscoda, Michigan. Groundwater Management Resources, Fall, 131-137.

Bevan M.J., Endres A.L., Rudolph D.L., Parkin G., 2005. A field scale study of pumping-induced drainage and recovery in an unconfined aquifer. Journal of Hydrology, 315(1-4), 52-70.

Brewster M.L., Annan A.P., 1994. Ground-penetrating radar monitoring of a controlled DNAPL release: 200 MHz radar. Geophysics, 59(8), 1211-1221.

Cápiro N.L., Stafford B.P., Rixey W.G., Bedient P.B., Alvarez P.J.J., 2007. Fuel-grade ethanol transport and impacts to groundwater in a pilot-scale aquifer tank. Water Research, 41, 656-664.

Cassidy N.J., 2007. Evaluating LNAPL contamination using GPR signal attenuation analysis and dielectric property measurements: Practical implications for hydrological studies. Journal of Contaminant Hydrology, 94, 49-75.

Che-alota V., Atekwana E.A., Atekwana E.A., Sauck W.A., Werkema Jr. D.D., 2009. Case History; Temporal geophysical signature from contaminant-mass remediation. Geophysics, 74(4), B113-B123.

Conant, B., 1991. Field studies of vertical well-screen placement: effect on recovery of stratified contaminants from an unconfined aquifer. M.Sc. Thesis, University of Waterloo, Waterloo, Ontario, Canada.

Corseuil, H.X., B.I.A. Kaier, and M. Fernandes. 2004. Cosolvency effect in subsurface systems contaminated with petroleum hydrocarbons and ethanol. Water Research, 38(6), 1449-1456.

Daniels J.J., 2004. Ground penetrating radar, 2nd Edition. The Institution of Electrical Engineers.

Daniels J.J., Roberts R., Vendl M., 1995. Ground penetrating radar for the detection of liquid contaminants. Journal of Applied Geophysics, 33, 195-207.

DeRyck, S.M., Redman, J.D., Annan, A.P., 1994. Geophysical monitoring of a controlled kerosene spill. Proceedings of the Symposium on the Application of Geophysics to Engineering and Environmental Problems (SAGEEP), San Diego, CA, 5–19.

Domenico, P.A., Schwartz, F.W., 1998. Physical and chemical hydrogeology. John Wiley & Sons, New York.

Freitas J.G., 2009. Impacts of ethanol in gasoline on subsurface contamination. Doctor of Philosophy Thesis. University of Waterloo, 1-269.

Freitas J.G., Barker J.F., 2011. Monitoring lateral transport of ethanol and dissolved gasoline compounds in the capillary fringe. Ground Water Monitoring & Remediation, 31, 95-102.

Freitas J.G., Doulatyari B., Molson J.W., Barker J.F., 2011. Oxygenated gasoline release in the unsaturated zone, Part 2: Downgradient transport of ethanol and hydrocarbons. Journal of Contaminant Hydrology, 125, 70-85.

Freyberg D.L., 1986. A natural gradient experiment on solute transport in a sand aquifer 2. Spatial moments and the advection and dispersion of nonreactive tracers. Water Resources Research, 22(13), 2013-2046.

Glaser, D. R., Henderson, R., Versteeg, R. J., Werkema, D. D., Kinoshita, R., Mattson, E., 2010. "Automated time-lapse GPR imaging of an ethanol release", Abstract H23C-1197 presented at 2010 Fall Meeting, AGU, SanFrancisco, Calif. 13-17 Dec.

Henderson, R., Werkema, D. D. Horton, R., Lane, J. W., 2009, Broadband geoelectrical signature of water-ethanol solutions in Ottawa Sand, Eos Trans. AGU, 90(53), Fall Meet. Supl., Abstract NS23A-1133

Henderson, R., Glaser, D. R., Johnson, T. C., Werkema, D. D. Versteeg, R. J., Lane, J. W., 2010, Time-lapse geoelectrical imaging of a controlled ethanol release in Ottawa Sand, Eos Trans. AGU, 91(53), Fall Meet. Supl., Abstract H13G-07

Jordan T.E., Baker G.S., Henn K., Messier J, 2004. Using amplitude variation with offset and normalization residual polarization analysis of ground penetrating radar data to differentiate an NAPL release from stratigraphic changes. Journal of Applied Geophysics, 56, 41-58.

Kim C., Daniels J.J., Guy E.D., Radzevichius S.J., Holt J., 2000. Residual hydrocarbons in a water-saturated medium: A detection strategy using ground penetrating radar. Environmental Geosciences, 7(4), 169-176.

Jones J.P., Sudicky E.A., Brookfield A.E., Park Y.J., 2006. An assessment of the tracer-based aroach to quantifying groundwater contributions to streamflow. Water Resources Research, 42(2), W02407.

Lucius, J.E., Olhoeft, G.R., Hill, P.L., Duke, S.K., 1992. Properties and hazards of 108 selected substances. U. S. Geological Survey Open File, 92-0527.

Lopes de Castro D., Branco R.M.G.C., 2003. 4-D ground penetrating radar monitoring of a hydrocarbon leakage site in Fortaleza (Brazil) during its remediation process: a case history. Journal of Applied Geophysics, 54, 127-144.

Mackay D.M., Freyberg D.L., Roberts P.V., Cherry J.A., 1986. A natural gradient experiment on solute transport in a sand aquifer 1. Approach and overview of plume movement. Water Resources Research, 22(13), 2017-2029.

Mackay D.M., De Sieyes N.R., Einarson M.D., Feris K.P., Paas A.A., Wood I.A., Jacobson L., Justice L.G., Noske M.N., Scow K.M., Wilson J.T., 2006. Impact of ethanol on the natural attenuation of benzene, toluene, and o-xylene in a normally sulfate-reducing aquifer. Environmental Science Technology, 40, 6123-6130.

McDowell C.J., Buscheck T., Powers S.E., 2003. Behaviour of gasoline pools following a denatured ethanol spill. Ground Water, 41(6), 746-757.

McDowell C.J., Powers S.E., 2003. Mechanisms affecting the infiltration and distribution of ethanol-blended gasoline in the vadose zone. Environmental Science Technology, 37, 1803-1810.

McNaughton C. H., 2011. Monitoring a shallow gasoline release using GPR at CFB Borden, M.Sc. thesis, University of Waterloo.

Mocanu M.T., 2006. Behaviour of oxygenates and aromatic hydrocarbons in groundwater from gasoline residuals. Masters of Science Thesis, University of Waterloo.

Nwankwor, G.I., 1982. A comparative study of specific yields in a shallow unconfined aquifer. MSc Thesis, University of Waterloo, Ont., Canada.

Nwankwor G.I., Gillham R.W., Vanderkamp G., Akindunni F.F., 1992. Unsaturated and saturated flow in response to pumping of an unconfined aquifer - Field evidence of delayed drainage. Ground Water, 30(5), 690-700.

O'Hannesin S.F., Gillham R.W., 1998. Long-term performance of an in situ "iron wall" for remediation of VOCs. Ground Water, 36(1), 164-170.

Orlando L., 2002. Detection and analysis of LNAPL using the instantaneous amplitude and frequency of ground-penetrating radar data. Geophysical Prospecting, 50, 27-41.

Parker J.C. 1989. Multiphase flow and transport in porous-media. Reviews of Geophysics, 27(3), 311-328.

Powers S.E., Hunt C.S., Heermann S.E., Corseuil H.X., Rice D., Alvarez P.J.J., 2001. The transport and fate of ethanol and BTEX in groundwater contaminated by gasohol. Critical Reviews in Environmental Science and Technology, 31(1), 79-123.

Redman, J. D., 2009. Chapter 8: Contaminant Mapping, *in* Jol H.M (editor), Ground penetrating radar: Theory and applications. Elsevier, Amsterdam, NL. 3 – 40.

Rice D.W., Powers S.E., Alvarez P.J.J., 1999. *Chapter 1:* Potential scenarios for ethanol-containing gasoline released into surface and subsurface waters. Volume 4: Potential Ground and Surface Water Impacts.

Rivett M.O., Feenstra S., Cherry J.A., 2001. A controlled field experiment on groundwater contamination by a multicomponent DNAPL: creation of the emplaced-source and overview of dissolved plume development. Journal of Contaminant Hydrology, 49, 111-149.

Ryan R.G. and Dhir V.K., 1996. The effect of interfacial tension on hydrocarbon entrapment and mobilization near a dynamic water table. Journal of Soil Contamination, 51, 9-34.

Sauck W.A., Atekwana E.A., Nash M.S., 1998. High conductivities associated with an LNAPL plume imaged by integrated geophysical techniques. Journal of Environmental and Engineering Geophysics, 2(3), 203-212.

Steelman, C. M., and Endres, A. L., 2009. Evolution of high-frequency ground-penetrating radar direct ground wave propagation during thin frozen soil layer development, Cold Regions Science and Technology, 57(2-3), 116-122.

Steelman, C. M., Endres, A. L., and van der Kruk, J., 2010. Field observations of shallow freeze and thaw processes using high-frequency ground-penetrating radar. Hydrological Processes, 24(14), 2022-2033.

Sudicky E.A., 1986. A natural gradient experiment on solute transport in a sand aquifer: Spatial variability of hydraulic conductivity and its role in the dispersion process. Water Resources Research, 22(13), 2069-2082.

Sudicky, E. A., and Illman, W. A., 2011. Lessons learned from a suite of CFB Borden experiments, Ground Water, 49(5), 630-648.

Werkema Jr. D.D., Atekwana E.A., Endres A.L., Sauck W.A., Cassidy D.P., 2003. Investigation the geoelectrical response of hydrocarbon contamination undergoing biodegradation. Geophysical Research Letters, 30(12), 49 1-4.

Woodbury A.D., Sudicky E.A., 1991. The geostatistical characteristics of the Borden aquifer. Water Resources Research, 27(4), 5333-546.

Yu S., Freitas J.G., Unger A.J.A., Barker J.F., Chatzis J., 2009. Simulating the evolution of an ethanol and gasoline source zone within the capillary fringe. Journal of Contaminant Hydrology, 105, 1-17.

Zhang Y., Khan I.A., Chen X., Spalding R.F., 2006. Transport and degradation of ethanol in groundwater. Journal of Contaminant Hydrology, 82, 183-194.

Appendix A (Folders Included in Attached Data Disk)

Material contained on the data disc can be obtained from the Department of Earth Sciences, upon request.

900 MHz Profiles

- Line A 900 MHz Profile Sequence
- Line B 900 MHz Profile Sequence
- Line C 900 MHz Profile Sequence
- Line D 900 MHz Profile Sequence
- Line E 900 MHz Profile Sequence
- Line 2 900 MHz Profile Sequence
- Line 3 900 MHz Profile Sequence
- Line 4 900 MHz Profile Sequence

450 MHz Profiles

- Line A 450 MHz Profile Sequence
- Line B 450 MHz Profile Sequence
- Line C 450 MHz Profile Sequence
- Line D 450 MHz Profile Sequence
- Line E 450 MHz Profile Sequence
- Line 2 450 MHz Profile Sequence
- Line 3 450 MHz Profile Sequence
- Line 4 450 MHz Profile Sequence

900 MHz CMP Soundings

- Line C 900 MHz CMP Centred at 1.0 m Sequence
- Line C 900 MHz CMP Centred at 3.2 m Sequence
- Line A 900 MHz CMP Centred at 3.2 m Sequence
- Line 4 900 MHz CMP Centred at 3.6 m Sequence
- Line E 900 MHz CMP Centered at 1.0m Sequence
- Trench 900 MHz CMP Centered at Middle Sequence

450 MHz CMP Soundings

- Line C 450 MHz CMP Centred at 1.0 m Sequence
- Line C 450 MHz CMP Centred at 3.2 m Sequence
- Line A 450 MHz CMP Centred at 3.2 m Sequence
- Line 4 450 MHz CMP Centred at 3.6 m Sequence
- Line E 450 MHz CMP Centered at 1.0m Sequence
- Trench 450 MHz CMP Centered at Middle Sequence

450 MHz Profile Traveltime contours
Soil Core Concentration Profiles
Frozen Ground Impedance Analysis
Pictures from Field Activities